Correction for LST directionality impact on the estimation of surface upwelling longwave radiation over vegetated surfaces at the satellite scale

Tian Hu, Jean-Louis Roujean, Biao Cao, Kaniska Mallick, Gilles Boulet, Hua Li, Zhihong Xu, Yongming Du, Qinhuo Liu

Remote Sensing of Environment 295 (2023) 113649

Contents lists available at ScienceDirect

Remote Sensing of Environment

journal homepage: www.elsevier.com/locate/rse

Correction for LST directionality impact on the estimation of surface upwelling longwave radiation over vegetated surfaces at the satellite scale

Tian Hu [a,*], Jean-Louis Roujean [c], Biao Cao [d], Kaniska Mallick [a,e], Gilles Boulet [c], Hua Li [d], Zhihong Xu [b], Yongming Du [d], Qinhuo Liu [d]

[a] Department of Environment Research and Innovation, Luxembourg Institute of Science and Technology, Belvaux 4362, Luxembourg
[b] Environmental Futures Research Institute, School of Environment and Science, Griffith University, Nathan, QLD 4111, Australia
[c] Centre d'Etudes Spatiales de la Biosphère, CNES, CNRS, INRA, IRD, UPS, Toulouse 31401, France
[d] State Key Laboratory of Remote Sensing Science, Aerospace Information Research Institute, Chinese Academy of Sciences, Beijing 100101, China
[e] Department of Environmental Science, Policy, and Management, University of California, Berkeley, CA 94720, United States

ARTICLE INFO

Edited by Jing M. Chen

Keywords:
LST
Thermal directionality
Parametric model
MODIS
SULR

ABSTRACT

Surface upwelling longwave radiation (SULR) is a major component of the Earth's radiation budget and directly influences the retrieval of evapotranspiration (ET) in the terrestrial ecosystems. Land surface temperature (LST) is an Essential Climate Variable (ECV) for direct estimation of SULR. However, accurate retrieval of SULR from satellite observations may be severely hindered by the anisotropic properties of land surface targets since most of them show marked angular variations in LST. This study aims at investigating the magnitude and impact factors of the directional effects of LST on SULR estimation over vegetated surfaces given that angular variation in emissivity has a limited impact on SULR estimation over most land surface types. It follows an attempt to correct for such effects in SULR estimation. We further explore the possibility to find a viewing direction at which SULR estimated from the directional LST can surrogate the hemispherical integration. To do so, a parametric model mimicking LST anisotropy with the hot spot is incorporated into the physical temperature-emissivity method. Two widely used Moderate Resolution Imaging Spectroradiometer (MODIS) LST products (i.e., MYD11_L2 and MYD21_L2) are analyzed. SULR estimates before and after correcting for LST directionality are compared with in-situ measurements acquired at 15 sites from the FLUXNET and SURFRAD networks in different regions. Our analysis reveals that LST directional effects on SULR estimation exhibit diurnal and seasonal variations, which are substantial in spring and summer for the daytime. The effects are negligible (<5 W m^{-2}) in autumn and winter for the daytime except for in arid and semiarid regions. For the night-time, the effects are insignificant over all the biomes. Using MYD21 LST, after correction, the average root-mean-square error (RMSE) and bias of SULR estimates for all sites decrease by 8 and 8.34 W m^{-2} in spring, and by 8.9 and 12.13 W m^{-2} in summer. Using MYD11 LST, after correction, the average RMSE is between 10 and 15 W m^{-2} and the average bias is close to zero in all seasons. The RMSE and absolute bias of SULR estimates for sites with low to moderate vegetation (LAI <3) is lowered substantially (7–14 W m^{-2}) after correction. Interestingly, SULR estimates from LST viewed at 54° backward and hemispherically integrated are close, with differences <3 W m^{-2} at most of the sites. These findings support a strategy for SULR estimation in ET retrieval over vegetated surfaces from directional LST.

1. Introduction

Surface upwelling longwave radiation (SULR) is defined as the sum of thermal radiation emitted by the land surface and the first-order reflected component of downward longwave radiation (DLR) from the atmosphere in the wavelength range of 4–100 μm (Cheng and Liang, 2016; Hu et al., 2017; Hu et al., 2016; Jiao et al., 2015; Wang and Liang, 2009). SULR represents the total upward thermal radiation flux at the Earth's land surface. It is influenced by multiple factors, notably incoming solar radiation, land cover type, soil moisture and topography, among others (Jiao et al., 2015; Liang et al., 2010; Wang and Liang, 2009, 2010). As a key component of surface radiation budget, SULR plays an important role in surface energy balance and directly influences the retrieval accuracy of evapotranspiration (ET) in the terrestrial

* Corresponding author.
E-mail address: tian.hu@list.lu (T. Hu).

https://doi.org/10.1016/j.rse.2023.113649
Received 31 July 2022; Received in revised form 8 May 2023; Accepted 23 May 2023
Available online 7 June 2023

ecosystems (Cheng and Liang, 2016; Hu et al., 2019b). It is found useful for a wide range of applications such as energy flux partitioning (Anderson et al., 2007; Mallick et al., 2018; Mallick et al., 2016; Trebs et al., 2021), agriculture water use (Hoffmann et al., 2016), drought monitoring (Hu et al., 2020a; Hu et al., 2020b), and global climate simulation (Trenberth and Fasullo, 2009).

Ground-based measurements of longwave radiation provide temporally continuous SULR data but with a very limited spatial coverage (Wang et al., 2012). Remote sensing observation is a reliable mean to obtain regional and global SULR mapping due to its large geographic coverage and public availability (Jiao et al., 2015; Wang et al., 2012). Several global SULR datasets are available, including the Global Energy and Water cycle Experiment-Surface Radiation Budget (GEWEX-SRB), the International Satellite Cloud Climatology Project-Flux Data (ISCCP-FD) and the Clouds and the Earth's Radiant Energy System-Gridded Radiative Fluxes and Clouds (CERES-FSW). Given the designed purpose for application in large-scale climate models, these SULR products generally have coarse spatial resolutions (100–280 km), and their accuracy at monthly timescale ranges between 21 and 34 W m^{-2} (Cheng and Liang, 2016). However, considering the acceptable accuracy of surface radiation retrievals for meteorological and other related uses ($<$ 20 W m^{-2} for instantaneous estimates and $<$ 10 W m^{-2} for monthly estimates (Ellingson, 1995; Gupta et al., 2004)), these SULR products do not meet the requirements and can generate large uncertainties in the subsequent applications (Cheng and Liang, 2016; Jiao et al., 2015; Wang et al., 2012). In addition, the coarse spatial resolutions will impede their usability in high spatial resolution (1–5 km) weather forecast, mesoscale land surface and atmospheric models due to the pronounced spatial heterogeneity of the land surface (Jiao et al., 2015; Wang and Liang, 2009). Thus, accurate SULR estimates at fine spatial resolution are highly desirable.

Various methods to estimate high-resolution SULR have been proposed. They can broadly be divided into two categories: physical temperature-emissivity method and empirical hybrid method (Cheng and Liang, 2016; Liang et al., 2019; Wang and Liang, 2009). The temperature-emissivity method takes advantage of land surface temperature (LST) and land surface emissivity (LSE) estimates based on satellite observations with moderate spatial resolutions such as Moderate Resolution Imaging Spectroradiometer (MODIS) and Visible Infrared Imaging Radiometer Suite (VIIRS) (Duan et al., 2019; Li et al., 2014; Li et al., 2019). SULR is estimated based on the Stefan-Boltzmann law. The hybrid method is based on an empirical relationship between SULR and the top-of-atmosphere (TOA) radiances issued from multivariate linear/nonlinear regression or artificial neural network (ANN). Separation of temperature and emissivity is bypassed by using TOA radiances directly. Wang and Liang (2009) evaluated the physical and empirical methods over the contiguous U.S. using the in-situ SULR measurement from the Surface Radiation Budget Network (SURFRAD, https://gml.noaa.gov/grad/surfrad/). It was reported that the clear-sky instantaneous SULR estimates using the temperature-emissivity method achieved an average root-mean-square error (RMSE) of 20.58 W m^{-2} and an average bias of −17.25 W m^{-2}. The multivariate linear regression method had an average RMSE of 17.63 W m^{-2} and an average bias of −10.46 W m^{-2}. The ANN method showed the highest accuracy, with RMSE of 15.23 W m^{-2} and bias of −7.94 W m^{-2}. At the opposite, Wu et al. (2012) compared the temperature-emissivity method and the linear regression method using a collection of ground-based measurements worldwide, and found that the physically-based temperature-emissivity method outperformed the linear method. Cheng and Liang (2016) developed the hybrid framework for estimating SULR over the globe by implicitly incorporating LST and air temperature difference after geographical division. The land surface was divided into low-, mid- and high-latitude regions based on LST and air temperature difference derived from the Atmospheric Infrared Sounder (AIRS) atmospheric profiles. They evaluated the linear and ANN methods under the proposed hybrid framework using in-situ SULR measurements from different observation networks and suggested that the linear regression method was more accurate than the ANN method, with a bias of −0.31 W m^{-2} and a RMSE of 19.92 W m^{-2}. Based on this proposed method, the Global Land Surface Satellite (GLASS, http://www.glass.umd.edu/Overview.html) longwave radiation product was generated and freely open to the public since 2018 (Liang et al., 2021; Cheng and Liang, 2016; Cheng et al., 2017), which provides the first high spatial resolution SULR dataset over the globe. The GLASS SULR product was reported to have a bias of −4.33 W m^{-2} and RMSE of 18.15 W m^{-2} (Zeng et al., 2020). Qin et al. (2020) comprehensively evaluated six different methods from both categories and found that the temperature-emissivity method using the MYD21 LST achieved the highest accuracy, with an RMSE of 14.0 W m^{-2} and a bias of −0.2 W m^{-2}, respectively, based on the estimates at the SURFRAD sites between 2017 and 2018. The accuracy was approximately 3 W m^{-2} higher as compared to those using the hybrid methods based on TOA radiances.

All the aforementioned methods may roughly satisfy the accuracy requirement for instantaneous clear-sky SULR. It remains that the thermal infrared (TIR) directional signature has been disregarded so far although the thermal directionality effects of the heterogeneous land surfaces can impact the estimation of longwave radiation emitted by the Earth's surface (Bian et al., 2020; Cao et al., 2019b). Several factors contribute to directional effects on a satellite TIR image. They are soil properties, vegetation structure, topography, mixed attributes (Cao et al., 2019b; Hu et al., 2019a; Yan et al., 2020). Thermal radiation directionality entails two components: the angular variation of LST and the emissivity directionality. The angular variation in satellite LST can reach ~9 K or more, depending on surface types and climate conditions (Coll et al., 2019; Hu et al., 2019a; Rasmussen et al., 2011; Rasmussen et al., 2010). Emissivity directionality varies with wavelength, with the most pronounced LSE difference between nadir and off-nadir (~0.03) around 8.55 μm over barren surfaces. It shows less significant angular variation in the two split-window channels centred around 11 and 12 μm (Hu et al., 2019b). Consequently, the angular variation of broadband emissivity is not pronounced because of the small linear weight (~0.3) for Band 29 in the calculation of broadband emissivity. Therefore, ignoring emissivity anisotropy does not impact the SULR estimation to a large extent (Hu et al., 2019b). Moreover, Cheng and Liang (2014) analyzed the influence of emissivity anisotropy (difference between directional and hemispherical broadband emissivities) on surface longwave radiation budget based on simulated and measured emissivity spectra. They reported that the maximum influence of emissivity angular variation was below 5.5 W^{-2} in all cases except for water and bare ice. In this case, considering LST directionality over vegetated surfaces is the major study focus here, which appears necessary for accurate retrieval of SULR and subsequent ET in the terrestrial ecosystems. Otterman et al. (1995) analyzed the relationship that exists between directional and hemispherical longwave radiations for a sparse canopy represented as thin, vertical cylindrical stalks laying over horizontal facets. Results of the simulation analysis revealed that looking at a view zenith angle of 50° is appropriate for estimating the hemispherical longwave emission. However, variations in the longwave emissions due to the viewing azimuth angle were not addressed although a strong azimuthal dependence exists due to the occurrence of the hot spot phenomenon. More investigation is needed to confirm the existence of equivalent viewing direction for SULR estimation, which can rely on in-situ or satellite measurements.

SULR estimation methods considering thermal directionality were recently implemented (e.g., Hu et al., 2017; Hu et al., 2016). These methods were based on TIR kernel-driven model (KDM) Ross-Li with a best fit of the coefficients by the time airborne multi-angular observations were collected. In thermal spectrum, KDM coefficients may not only vary with the biophysical properties but also with factors describing the meteorological environment of the canopy (e.g., wind speed, humidity). Thus, they are not valid at another time. Moreover, as opposed to optical data, TIR date cannot be accumulated over time to

obtain a better calibration of KDM coefficients, even over very short periods of time. Thus, choosing a KDM with temporally quasi-invariant coefficients is essential for a broader applicable extent. In these proposed methods (Hu et al., 2017; Hu et al., 2016), angular variation in both emissivity and LST is considered via different means. Recently, it was shown that the anisotropy of emissivity has an insignificant influence on SULR estimation (Hu et al., 2019b). Therefore, LST directionality effects on SULR are of interest here. In the past two decades, three major KDM depicting directional LST have been extensively used under the assumption of temporally quasi-invariant model coefficients, i.e., the Roujean-Lagouarde (RL) model (Lagouarde and Irvine, 2008), the Vinnikov model (Vinnikov et al., 2012), and the Hotspot-Kernel model (Ermida et al., 2018b). The core for the temporal invariance assumption is the introduction of the nadir-viewing temperature, as opposed to the simple utilization of directional temperature in the Ross-Li model. Under this modeling scheme, the temporal variation of surface directional temperature is expressed in the nadir-viewing temperature, sun zenith angle and daily TOA radiation instead of the model coefficients. The TOA radiation introduces seasonal variability in LST directionality, and nadir-viewing temperature and sun zenith angle introduce the diurnal variation. Ermida et al. (2018a) calibrated these parametric models over the entire SEVIRI disk by combining the concurrent LST retrievals from the MODIS polar-orbiting and Spinning Enhanced Visible and Infrared Imager (SEVIRI) geostationary observations and extended the regressed model coefficients globally based on the 15 classified surface clusters. This provided an opportunity to incorporate the KDM into SULR estimation using satellite observations.

Herein, the objective is to evaluate the influence of LST directionality on SULR over vegetated surfaces at the satellite scale through the incorporation of a KDM mimicking LST anisotropy into the physically based temperature-emissivity method. Two MODIS LST products, i.e., MYD11_L2 and MYD21_L2, are considered. The SULR estimates are evaluated using in-situ measurements collected in different regions. The objectives of this study are twofold: (1) to investigate the magnitude and impact factors of LST directional effects on SULR estimation, and how to correct for these effects; (2) to identify a viewing direction at which SULR estimate is equivalent to its hemispherical integration. Overall, the study will serve as a support for improving the accuracy of SULR estimation and subsequent ET retrieval in the terrestrial ecosystems.

2. Data

2.1. MODIS data

Two widely used MODIS LST products, i.e., MYD11_L2 and MYD21_L2 for Collection 6, were processed to estimate SULR separately for the two years of 2010 and 2011. Considering the possible crosstalk effect in Band 29 of the sensor onboard Terra, only data from Aqua were used in this study. The MYD11 LST data are obtained using the Generalized Split-Window (GSW) algorithm based on the different atmospheric absorptions in the two thermal bands centered around 11 and 12 μm (Wan, 2014; Wan and Dozier, 1996). The emissivities for the two split-window bands are estimated using a classification-based algorithm developed by Snyder et al. (1998). The MYD21 product is obtained using the Temperature Emissivity Separation (TES) algorithm that estimates LST and LSE simultaneously (Gillespie et al., 1998; Hulley et al., 2016). TOA brightness temperatures in three thermal bands centered 8.55, 11 and 12 μm are used in the TES algorithm. LSEs in these three bands are provided in the MYD21 product. The MYD03 products were used to provide the geospatial information for other MODIS products. All the MODIS products used here have a spatial resolution of 1 km and two revisits (day and night) per day.

2.2. Model coefficients

By using the collocated LST retrievals from MODIS (onboard both Aqua and Terra, Collection 5) and SEVIRI covering the full year of 2011, Ermida et al. (2018a) calibrated the KDM models under the assumption that their coefficients remain temporally invariant (at least within one season or a year). After spatial and temporal collocation, systematic differences between MODIS and SEVIRI LST products were removed by a linear adjustment of MODIS LST. The collocated night-time LST data were used to calculate a model coefficient first while the other coefficients were estimated using the collocated daytime LST. From their knowledge over Europe, Africa and part of South America, an extrapolation scheme over the globe was further applied after clustering landscape units based on the following criteria: surface elevation, land cover type, fraction of vegetation cover (FVC). The calibrated KDM models were evaluated using both the calibration database over the SEVIRI disk and an independent database composed of matchups between MODIS and various geostationary satellite LST products in different regions over the globe. Results showed that the difference between MODIS and geostationary satellite LST decreased by 1.1 K on average after angular correction using the calibrated KDM models and changes were as high as 5.5 K. Moreover, the decrease was consistent over the globe. More details can be found in the study by Ermida et al. (2017). Here, KDM coefficients for the globe were obtained directly from Sofia L. Ermida and Isabel F. Trigo (pers. comm., 2019), with a spatial resolution of $0.05^\circ \times 0.05^\circ$.

2.3. Ground measurements

In-situ radiation measurements were collected in different regions. In total, 15 sites were selected from different measurement networks (Table 1), covering six land surface types including evergreen needleleaf

Table 1
Validation sites used in this study.

Site No.	Site ID*	Latitude	Longitude	Elevation (m)	Land cover type
1	NR1[a]	40.0329° N	105.5464° W	3050	Evergreen needleleaf forests
2	SRM[a]	31.8214° N	110.8661° W	1120	Woody savannas
3	UMB[a]	45.5598° N	84.7138° W	234	Deciduous broadleaf forests
4	Wkg[a]	31.7365° N	109.9419° W	1531	Grassland
5	Ses[a]	34.3349° N	106.7442° W	1604	Open shrubland
6	Ne3[a]	41.1797° N	96.4397° W	363	Cropland
7	SRC [a]	31.9083° N	110.8395° W	950	Open shrubland
8	BND[b]	40.0519° N	88.3731° W	230	Cropland
9	TBL[b]	40.1250° N	105.2368° W	1689	Grassland
10	DRA[b]	36.6237° N	116.0195° W	1007	Open shrubland
11	FPK[b]	48.3078° N	105.1017° W	634	Grassland
12	Lnf[c]	51.3282° N	10.3678° E	451	Deciduous broadleaf forests
13	Lkb[c]	49.0996° N	13.3047° E	1308	Evergreen needleleaf forests
14	Das[d]	14.1592° S	131.3881° E	110	Woody savannas
15	ASM[d]	22.2828° S	133.2493° E	606	Woody savannas

[a]AmeriFlux sites; [b]SURFRAD sites; [c]EFDC sites; [d]OzFlux sites.

* NR1: Niwot Ridge Forest, SRM: Santa Rita Mesquite, UMB: Univ. of Mich. Biological Station, Wkg: Walnut Gulch Kendall Grasslands, Ses: Sevilleta shrubland, Ne3: Nebraska Mead - Rainfed Maize-soybean Rotation Site, SRC: Santa Rita Creosote, BND: Bondville, TBL: Table Mountain, DRA: Desert Rock, FPK: Fort Peck, Lnf: Leinefelde, Lkb: Lackenberg, Das: Daly River Uncleared, ASM: Alice Springs Mulga.

forests, woody savannas, deciduous broadleaf forests, cropland, grassland, open shrubland. The spatial distribution of the 15 sites is shown in Fig. 1, encompassing four sites from the Surface Radiation Budget (SURFRAD) network, seven sites from the AmeriFlux network, two sites from the European Fluxes Database Cluster (EFDC) network, and two sites from the OzFlux network. The temporal frequencies of acquisition for the SURFRAD and AmeriFlux/EFDC/OzFlux data sets are 1 and 30 min(s), respectively. These sites were selected due to the homogeneity of surrounding landscapes and their various land surface types (Cheng and Liang, 2016; Guillevic et al., 2018; Wang et al., 2008; Duan et al., 2019).

3. Methodology

3.1. Parametric model for LST angular variation

Worth recalling that three parametric models are retained: RL model, Vinnikov model and Kernel-Hotspot model. The coefficients of these models were calibrated at the satellite scale in the full year of 2011, during which they were assumed invariant (Ermida et al., 2018a).

RL model proposed by Lagouarde and Irvine (2008) was obtained via substituting reflectance for LST in the optical hot spot model developed by Roujean (2000). However, RL model cannot be used to estimate directional LST during the night-time as it is designed to consider LST directionality caused by solar illumination and viewing geometry. It also showed poor performances over surfaces with low tree coverage (Ermida et al., 2018a; Ermida et al., 2018b).

Vinnikov model proposed by Vinnikov et al. (2012) includes an isotropic term, an emissivity kernel and a solar kernel. Duffour et al. (2016) evaluated the Vinnikov model using a simulation dataset. The Vinnikov model was reported to underperform the RL model overall, especially at directions close to the hot spot where the Vinnikov model failed. This was also confirmed by Cao et al. (2019a).

By combining the assets of the RL model and the Vinnikov model, Ermida et al. (2018b) proposed the Kernel-Hotspot model, expressed as

$$T_s(\theta,\theta_i,\varphi) = T_0 + AT_0\Phi(\theta) + BRad_{TOA}sin(2\theta_i)\frac{e^{-kd} - e^{-ktan\theta_i}}{1 - e^{-ktan\theta_i}} \quad (1)$$

where θ, θ_i and φ are viewing zenith angle, solar zenith angle and relative azimuth angle, respectively, T_s is the directional LST, T_0 is the LST viewed from the nadir direction, $\Phi(\theta)$ is the same emissivity kernel as in the Vinnikov model $1 - cos(\theta)$, the second term at the right side is the Hotspot kernel modified based on the RL model, Rad_{TOA} is the daily TOA radiation normalized by the daily solar constant (Meeus, 1991), A, B and k are model coefficients, d is the angular distance between the sun and viewing positions defined as:

$$d = \sqrt{tan^2\theta_i + tan^2\theta - 2tan\theta_i tan\theta cos\varphi}. \quad (2)$$

The Kernel-Hotspot model was demonstrated to outperform both the RL model and Vinnikov model, with improved performance during night-time and for low tree densities (Ermida et al., 2018b). Cao et al. (2021) reported that the Kernel-Hotspot model showed an RMSE of ~0.2 K in the evaluation using both model simulation (4SAIL and DART) and airborne multi-angular data over continuous and discrete canopies by comparing the evaluation data and the simulations from the Kernel-Hotspot model at different viewing geometries. Moreover, due to the introduction of T_0 in the Kernel-Hotspot model, the temporal dynamics in model coefficients are removed. Therefore, it was decided to consider the Kernel-Hotspot model to describe LST directionality in this study. Note that the Hotspot kernel is irrelevant for the night-time and that the corresponding kernel coefficient (B) is set to zero. Since the model coefficients were a priori known thanks to their global calibration (Section 2.2), the only unknown variable, i.e., T_0, was calculated from MODIS LST $T_s(\theta,\theta_i,\varphi)$ and the parametric models. This served to derive the

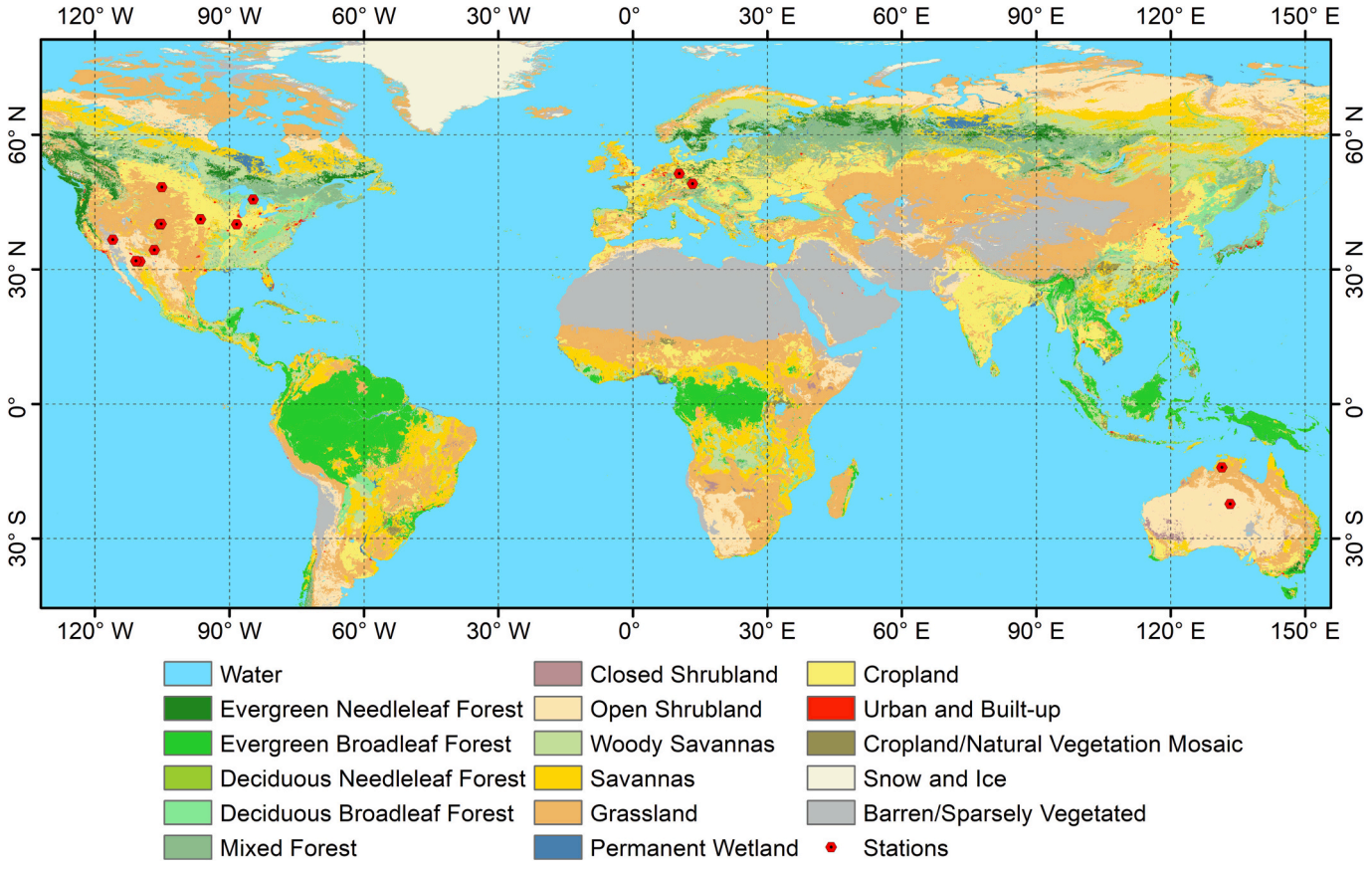

Fig. 1. Spatial distribution of the validation sites. The background is the land surface classification from the MCD12C1 product of 2010.

directional LST at any viewing angle from the parametric model.

3.2. SULR estimation incorporating LST angular variation

When LST angular variation is incorporated, SULR can be expressed as

$$SULR = \varepsilon \int_0^{2\pi} \int_0^{\pi/2} \int_{\lambda_1}^{\lambda_2} B_\lambda(T_s(\theta,\theta_i,\varphi))d\lambda cos(\theta)sin(\theta)d\theta d\varphi + (1-\varepsilon)DLR \quad (3)$$

where ε is the surface broadband emissivity (BBE), B_λ is the Planck function, λ_1 and λ_2 are the spectral range for SULR estimation (4–100 μm), $T_s(\theta,\theta_i,\varphi)$ is the land surface directional effective temperature, and DLR is the downwelling longwave radiation. Based on the Stefan-Boltzmann law specifying that the total energy radiated per unit surface area of a black body in unit time is proportional to the fourth power of the black body's temperature, Eq. (3) can be transformed to

$$SULR = \frac{\varepsilon\sigma}{\pi} \int_0^{2\pi} \int_0^{\pi/2} T_s{}^4(\theta,\theta_i,\varphi)cos(\theta)sin(\theta)d\theta d\varphi + (1-\varepsilon)DLR \quad (4)$$

where σ is the Stefan-Boltzmann constant (5.67×10^{-8} W m^{-2} K^{-4}).

In this case, BBE, DLR and directional temperature are the required input parameters. Here, BBE was calculated using the band-effective emissivities in MODIS bands 29 (~8.55 μm), 31 (~11 μm) and 32 (~12 μm) from the MYD21 product as follows (Wang et al., 2005):

$$\varepsilon_{bb} = 0.2493\varepsilon_{29} + 0.4447\varepsilon_{31} + 0.3088\varepsilon_{32} \quad (5)$$

where ε_{bb} is the BBE, ε_{29}, ε_{31} and ε_{32} are the emissivities in MODIS Bands 29, 31 and 32, respectively. DLR was directly obtained from the in-situ measurements considering that the goal here is to focus on LST and its angular variation and that considering ground-truth DLR better supports the analysis. Moreover, the influence of uncertainties in DLR on SULR estimation is insignificant considering the reflectance (1 - ε) is below 0.05 for most surfaces and the uncertainties in DLR are normally within 30 W m^{-2} (Yu et al., 2022). We estimate the directional temperatures over the upper hemisphere with a bin of 1° for the zenith and azimuth angles from the instantaneous MODIS LST (either the MYD11 or MYD21 LST data) based on the Kernel-Hotspot model. Then, SULR is calculated using the BBE, DLR and the directional temperatures in different directions over the upper hemisphere based on Eq. (3). The integral calculation is conducted using the trapezoid rule to approximate the analytical solution.

3.3. Evaluation method

SULR estimates with and without correcting for LST directional effects were evaluated using the in-situ measurements. The two MODIS LST products, namely MYD11 and MYD21, were considered separately. Also, the estimates in the four seasons and for daytime and night-time were distinguished in this evaluation.

In the evaluation, the "3σ-Hampel identifier" outlier removal method proposed by Davies and Gather (1993) was adopted to remove the outliers in the SULR estimates caused by undetected cloud contamination in LST retrieval (Duan et al., 2019; Göttsche et al., 2013). In this method, the standard deviation is estimated as.

$$S = 1.4826 \times median(|x_i - x_m|) \quad (6)$$

where S is the standard deviation, x_m is the median of the data sequence $[x_i]$. Here, $[x_i]$ is the difference between the estimated SULR and in-situ measurements. The samples with SULR differences $< x_m$-3S or $> x_m + 3S$ were regarded as outliers and excluded for further analysis.

Three statistical indicators, i.e., RMSE, bias, and relative RMSE (RRMSE), were used to quantify the accuracy of SULR estimates before and after correcting for LST directionality. These indicators were calculated as

$$RMSE = \sqrt{\frac{\sum (SULR_{sat,i} - SULR_{insitu,i})^2}{N}} \quad (7)$$

$$bias = mean(SULR_{sat,i} - SULR_{insitu,i}) \quad (8)$$

$$RRMSE = \sqrt{\frac{\sum (SULR_{sat,i} - SULR_{insitu,i})^2}{\sum SULR_{sat,i}{}^2}} \quad (9)$$

where $SULR_{sat,i}$ and $SULR_{insitu,i}$ are the SULR estimates from the MODIS data and in-situ measurements, respectively.

In this study, the accuracy of the SURFRAD measurements (5 W m^{-2}, https://gml.noaa.gov/grad/surfrad/overview.html) was used as a criterion to determine whether the improvement after correcting for LST directionality is significant or not. The improvement was regarded as negligible if the improvement is below 5 W m^{-2} considering the difficulty to distinguish the improvement from the measurement uncertainty.

3.4. Searching for an equivalent viewing angle

The equivalent viewing angle is defined here as the observation geometry at which SULR calculated using the directional LST can surrogate the hemispherical integration without introducing significant uncertainties. To assess the quality of the equivalence between the directional estimate and the hemispherical estimate, the Kling-Gupta efficiency (KGE) is adopted. As a measure of the goodness-of-fit, KGE provides a quantitative and objective assessment of the agreement between observed and simulated data (Gupta et al., 2009). It is calculated as

$$KGE = 1 - \sqrt{(r-1)^2 + \left(\frac{\sigma_s}{\sigma_0} - 1\right)^2 + \left(\frac{u_s}{u_0} - 1\right)^2} \quad (10)$$

where r is the Pearson correlation coefficient, σ_0 and σ_s are the standard deviations of observations and simulated values, respectively, and u_0 and u_s are the averages of observations and simulated values, respectively. Herein, the hemispherical and directional estimates are regarded as the reference and proxy values, respectively. The optimization problem can then be expressed as a problem of finding the right viewing angle where the KGE peaks, viz.:

$$\Omega = argmax[KGE(\Omega)] \quad (11)$$

where Ω is the viewing geometry.

4. Results and analysis

4.1. Simulation analysis

A simulation was performed first to analyze how the seasonal and diurnal changes of LST directionality yield an impact on SULR estimates. We selected three sites (i.e., Ses, BND, and UMB) from Table 1 with different land cover types encompassing desert grassland, cropland, and broadleaf forest. These three sites represent barren, intermediately vegetated, and densely vegetated surfaces, respectively, which cover a gradient of vegetation coverage. Then, we simulated the directional LST over the upper hemisphere in different seasons and for daytime and night-time using the calibrated Kernel-Hotspot model and the MYD21 LST data (8 estimates, in four seasons and for both day and night). Differences between SULR estimates using directional satellite LST estimate and via hemispherical integration of LST based on Eq. 4 were calculated. Results are exemplified in Figs. 2 and 3.

The angular variation for the daytime is much more pronounced in

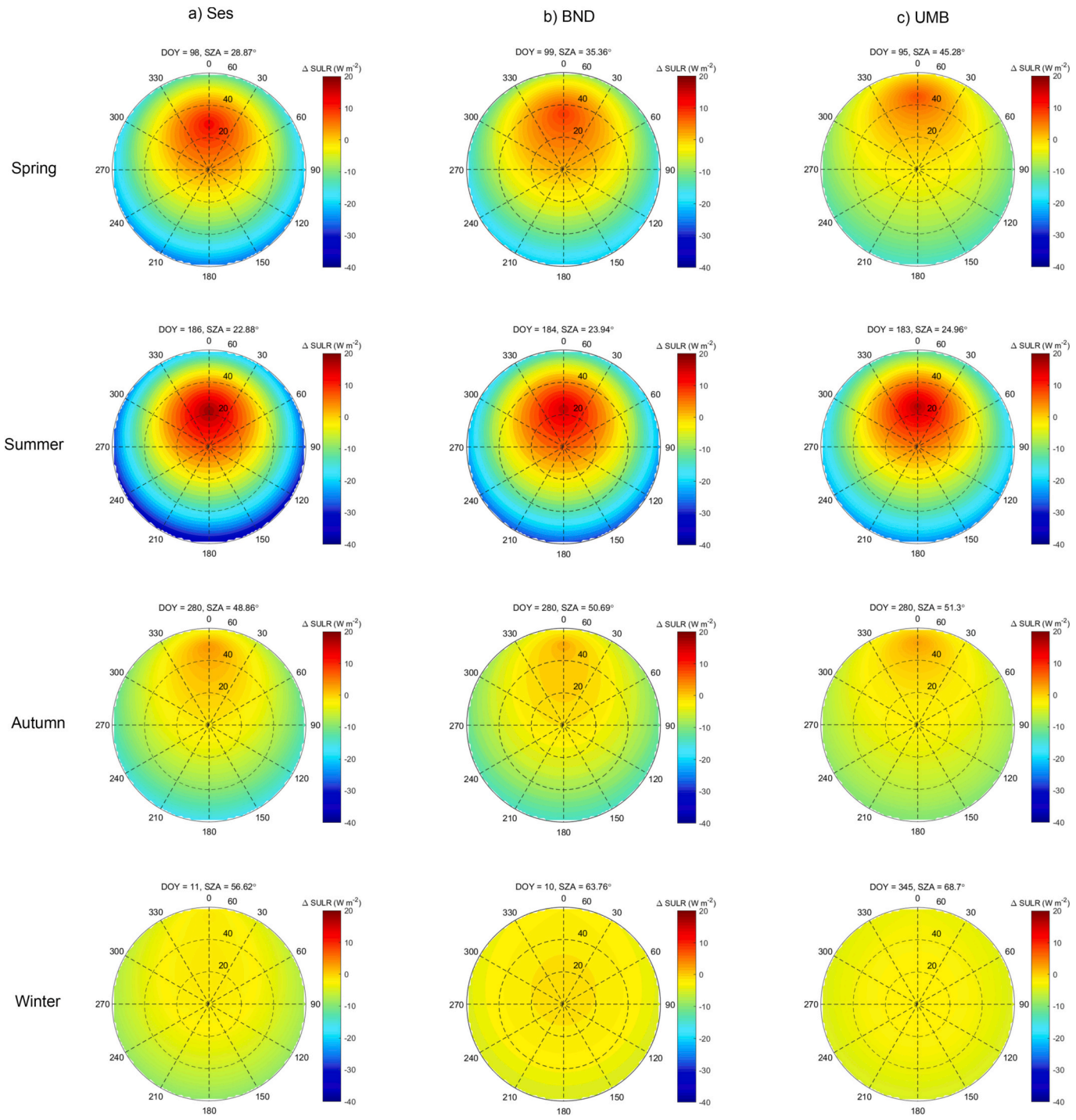

Fig. 2. Difference between SULR estimates using directional LST and via hemispherical integration of LST at (a) Ses, (b) BND and (c) UMB for the daytime. The MYD21 LST data were used to adjust the Kernel-Hotspot model. The magnitude and phase angle represent VZA and relative azimuth angle (RAA), respectively. SZA indicates the illumination condition at the MODIS overpass time.

spring and summer than in autumn and winter, with the strongest directionality occurring in summer. The SULR estimate from directional LST is significantly larger than the hemispherical estimate when the observation angle is close to the sun illumination angle (~20 W m^{-2} at Ses in summer), and remarkably lower than the hemispheric estimate when viewing zenith angle (VZA) approaches 60° in the forward scattering direction (~40 W m^{-2} at Ses in summer). The SULR estimated using the directional LST at a VZA angle between 40° and 60° in the back-scattering direction in the principal plane is close to the hemispherical estimate, which is obvious in spring and summer. For the night-time, the angular variation is minor. In this case, thermal directionality is depicted only by the emissivity kernel.

Among the three land cover types, the Ses site covered by mixed-species desert grassland shows the most pronounced angular variation. While the BND site (cropland) reveals the intermediate thermal directionality, the UMB site (densely vegetated forest) exhibits the weakest directionality, which is typical for a homogeneous landscape.

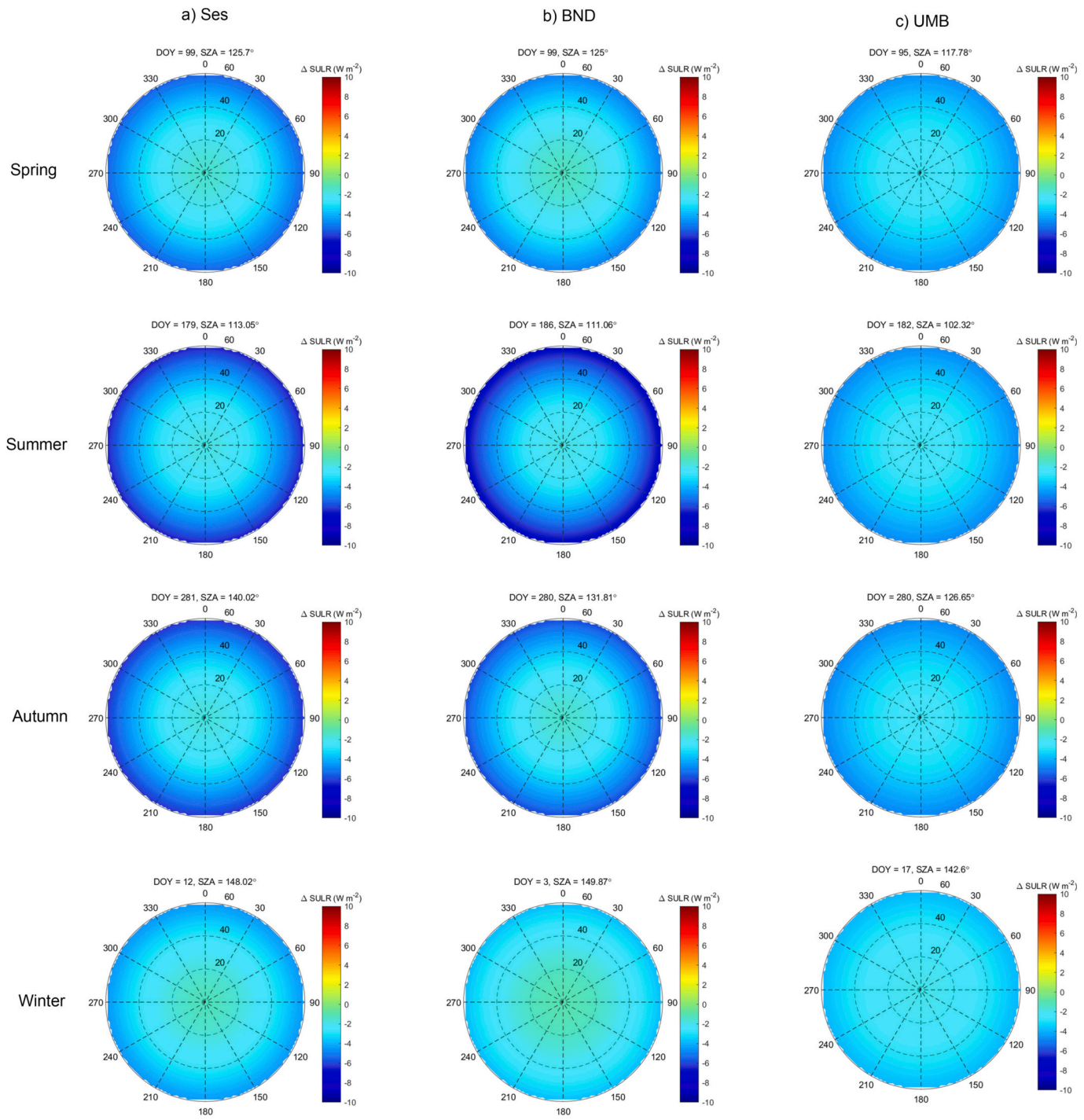

Fig. 3. Id. Fig. 2 for nighttime.

4.2. Evaluation of the results using in-situ measurements

The results of evaluation for different seasons and daytime are shown in Figs. 4 and 5. The cases with sample numbers below 20 are discarded from the analysis. It comes out that the RMSE and absolute biases in spring and summer are significantly greater than in autumn and winter. The average RMSE among all the sites in spring and summer is around 20 W m^{-2}. Whereas the average RMSE in autumn and winter is ~10 W m^{-2}. The pattern is the same over both the Northern and Southern Hemispheres. This is attributed to the existence of higher temperatures and more thermal heterogeneity in the pixels in spring and summer. Since the path of the sun is enhanced, more thermal gradients are observed, which means more pronounced thermal directionality.

Compared with the SULR estimates issued from standard MYD21 LST (referred to as MYD21 in Figs. 4 and 5), SULR derived with a correction for LST directionality using the Kernel-Hotspot model (MYD21_KH) shows a pronounced decrease in RMSE and absolute bias in spring and summer, which are on average 8 and 8.34 W m^{-2} for RMSE and bias, respectively, in spring (see Table 2). These statistics become 8.9 and 12.13 W m^{-2} in summer (see Table 3). The improvement of SULR estimates after correcting LST directionality in autumn and winter is marginal (<5 W m^{-2}) due to the relatively low temperature and reduced shadowing effect except for over woody savannas and open shrubland. In these arid and semiarid regions, the emissivity kernel in the LST

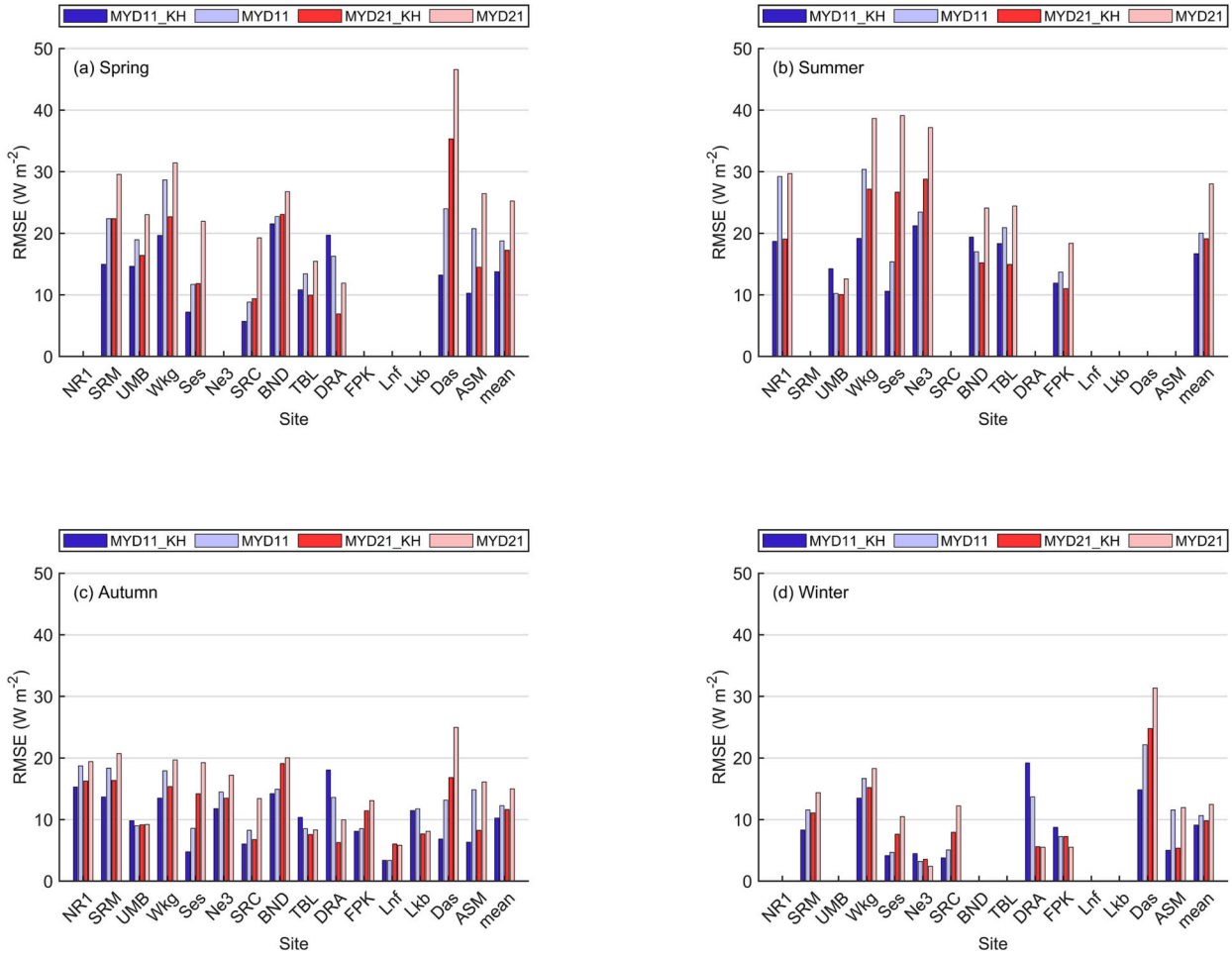

Fig. 4. RMSE of the SULR estimates in (a) spring, (b) summer, (c) autumn and (d) winter for the daytime. MYD11_KH and MYD11 represent the SULR estimate obtained from the MYD11 LST data after correcting for LST directionality based on the Kernel-Hotspot model and that obtained directly using the MYD11 LST retrieval, respectively. MYD21_KH and MYD21 represent the SULR estimate obtained from the MYD21 LST data after correcting for LST directionality based on the Kernel-Hotspot model and that obtained directly using the MYD21 LST retrieval, respectively.

directionality model plays an important role due to the substantial proportion of bare soil in the landscape although the shadowing effect is less significant in autumn and winter. The temperature in autumn and winter is also relatively higher as compared to those over other biomes.

Also, an improvement is obtained for the SULR estimates using the MYD11 LST after directional correction on LST (MYD11_KH) in spring and summer for most sites while being negligible in autumn and winter. SULR estimates after correction is similar for the two LST MODIS products (MYD21_KH and MYD11_KH). The MYD11_KH estimates have the lowest absolute bias at most sites among the four cases (i.e., MYD11_KH, MYD11, MYD21_KH, MYD21). The average RMSE of MYD11_KH is generally below 15 W m^{-2}, and the average bias is around zero in all seasons. However, at the site DRA, the RMSE and absolute bias of SULR estimates using the MYD11 LST are increased in all seasons after correcting LST directionality, being the largest among the four cases. Compared with the MYD21 LST, the MYD11 LST seems to be less impacted by LST directionality, which is exemplified by the smaller discrepancy between SULR estimates from MYD11 LST before and after correcting LST directionality in spring and summer. More investigations are needed to understand the different performances of the MYD21 and MYD11 LST data in SULR estimation considering LST directionality.

The improvement in spring and summer is more pronounced when the landscape is sparsely or moderately vegetated. For example, at the semiarid site Wkg (Ses) covered by sparse desert grassland (Fig. 6), the RMSE and absolute bias using the MYD21 LST decrease by 8.75 (10.09) and 7.53 (8.58) W m^{-2} in spring, and by 11.49 (12.44) and 10.68 (13.89) W m^{-2} in summer. Those using the MYD11 LST at the site Wkg (Ses) decrease by 9.00 (4.51) and 7.51 (1.56) W m^{-2} in spring, respectively, and by 11.20 (4.78) and 10.54 (6.89) in summer, respectively. This is very likely due to the anisotropy of the emissivity of bare soil, which propagates to LST retrievals for sparse canopies (Trigo et al., 2021). Comparison between an open evergreen needleleaf forest (site NR1) and a closed deciduous broadleaf forest (site UMB) for summertime (Fig. 6) reveals that more improvement is obtained for NR1 than for UMB, with a decrease of RMSE and bias of ~10 W m^{-2}. This could be attributed to the shadowing effect and contrasting heating for different endmembers within a pixel at the NR1 site. Moreover, the improvement at UMB (~6 W m^{-2} decrease in RMSE) is greater in spring than in summer (~2 W m^{-2} decrease in RMSE), likely because the canopy of the deciduous forest in spring is not closed yet and contrasting temperatures of trees and the ground increase the thermal directionality.

For the night-time (Figs. 7 and 8), the RMSE and absolute bias are much lower than for the daytime, with an average RMSE and absolute bias <10 W m^{-2} in all seasons. Also, the seasonal variation in RMSE and bias for the night-time is negligible as compared to that for the daytime. The improvement of the SULR estimates after incorporating LST directionality correction is not conspicuous at all sites. The RMSE and absolute bias are slightly increased at most sites. This could be attributed to the substantially weaker angular variation of LST during the night-time than during the daytime and more frequent thermal equilibrium in the

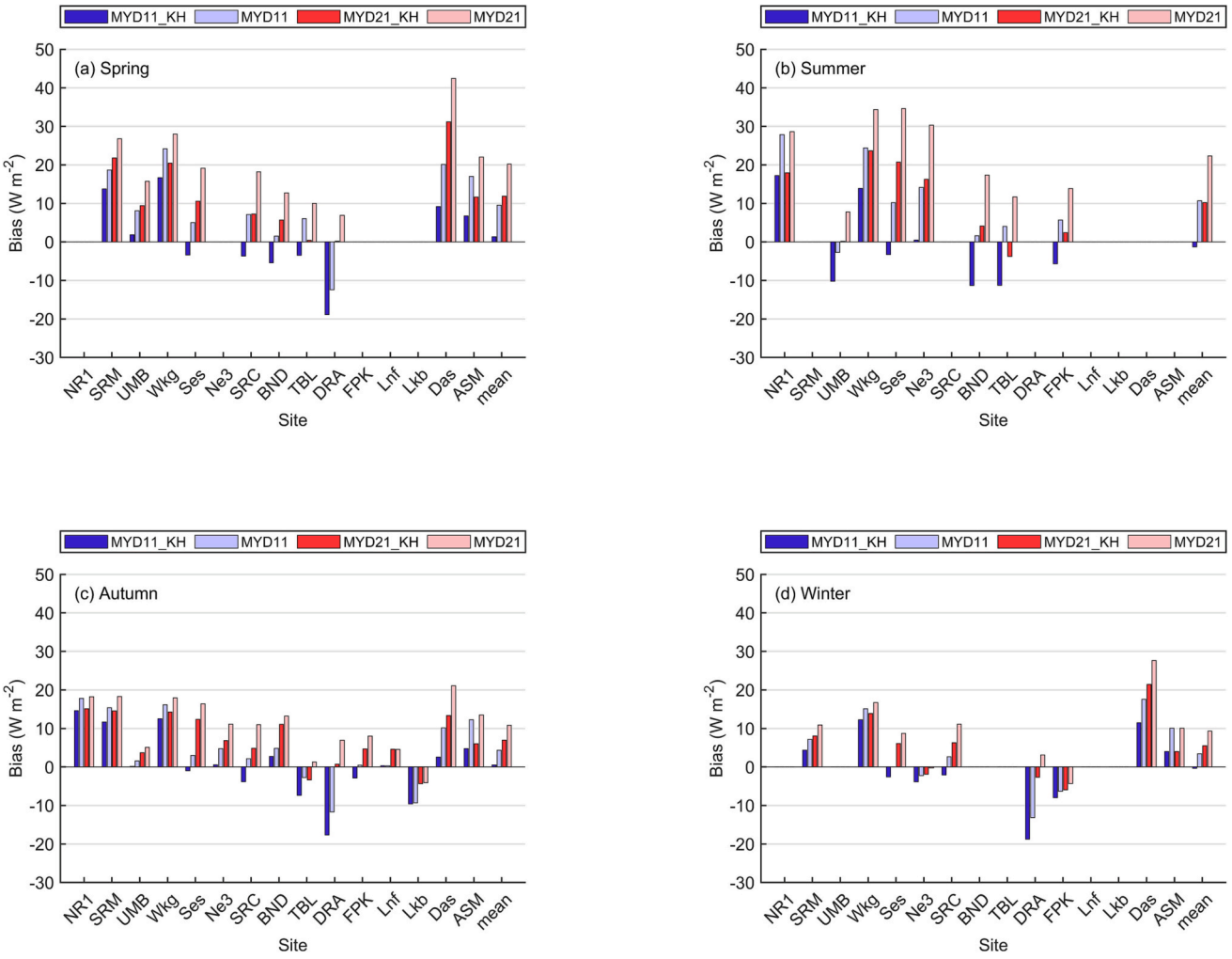

Fig. 5. Biases of the SULR estimates in (a) spring, (b) summer, (c) autumn and (d) winter for the daytime.

Table 2
Evaluation results of the four methods at different sites in spring for the daytime. The SULR estimates used in the evaluation were obtained by retaining the common ones retrieved from the four estimation methods after outlier removal.

Site	Sample Number	MYD11_KH		MYD11		MYD21_KH		MYD21	
		Bias	RMSE	Bias	RMSE	Bias	RMSE	Bias	RMSE
SRM	23	13.73	14.97	18.63	22.37	21.78	22.39	26.75	29.55
UMB	24	1.83	14.63	8.08	18.94	9.37	16.39	15.72	23.03
Wkg	108	16.65	19.65	24.16	28.65	20.45	22.67	27.98	31.42
Ses	79	−3.42	7.19	4.98	11.70	10.57	11.84	19.15	21.93
SRC	22	−3.65	5.71	7.10	8.83	7.24	9.38	18.21	19.25
BND	27	−5.42	21.53	1.49	22.71	5.67	23.04	12.70	26.76
TBL	23	−3.48	10.83	6.03	13.43	0.40	9.94	9.98	15.44
DRA	32	−18.88	19.69	−12.41	16.25	0.18	6.90	6.87	11.90
Das	24	9.18	13.22	20.14	23.98	31.15	35.30	42.45	46.58
ASM	36	6.74	10.25	16.98	20.76	11.65	14.49	22.03	26.44
Mean	–	1.33	13.77	9.52	18.76	11.85	17.23	20.19	25.23

lack of solar illumination. There is also a possibility of overfitting when the parametric model is used to correct the thermal directionally in this case even though the hotspot kernel is deactivated for the night-time.

At night and DRA site, the SULR estimates using the MYD21 LST show markedly lower RMSE and absolute bias values than those using the MYD11 LST. At other sites, statistical results are rather equivalent for MYD21 and MYD11 LST. Overall, a higher accuracy of SULR estimates is obtained using the MYD21 LST for the night-time.

To quantify the magnitude of thermal directionality, we propose to use the standard deviation of directional temperature in the principal plane. To get the threshold of the standard deviation that decides whether a correction for LST directionality is needed, we analyzed the conditions at all the sites. The standard deviation was calculated by sampling in the principal plane between −90° and 90° with a bin of 10°. As shown in Fig. A1, the threshold of 2.5 K could be used to determine whether the directionality correction is needed. During the daytime, most of the LST standard deviations are above 2.5 K in spring. In summer, almost all of the standard deviations are above 2.5 K. In autumn

Table 3
Same as Table 2 except the season is summer.

Site	Sample Number	MYD11_KH		MYD11		MYD21_KH		MYD21	
		Bias	RMSE	Bias	RMSE	Bias	RMSE	Bias	RMSE
NR1	24	17.21	18.68	27.86	29.23	17.94	19.03	28.61	29.68
UMB	40	−10.22	14.24	−2.73	10.22	0.16	10.05	7.79	12.59
Wkg	36	13.87	19.18	24.41	30.38	23.69	27.16	34.37	38.65
Ses	84	−3.28	10.59	10.17	15.37	20.69	26.67	34.58	39.11
Ne3	48	0.48	21.21	14.17	23.43	16.27	28.78	30.32	37.17
BND	29	−11.32	19.36	1.56	16.98	4.09	15.23	17.32	24.08
TBL	45	−11.26	18.32	4.00	20.92	−3.78	14.93	11.68	24.44
FPK	50	−5.67	11.92	5.65	13.70	2.38	11.03	13.83	18.35
Mean	–	−1.27	16.69	10.64	20.03	10.18	19.11	22.31	28.01

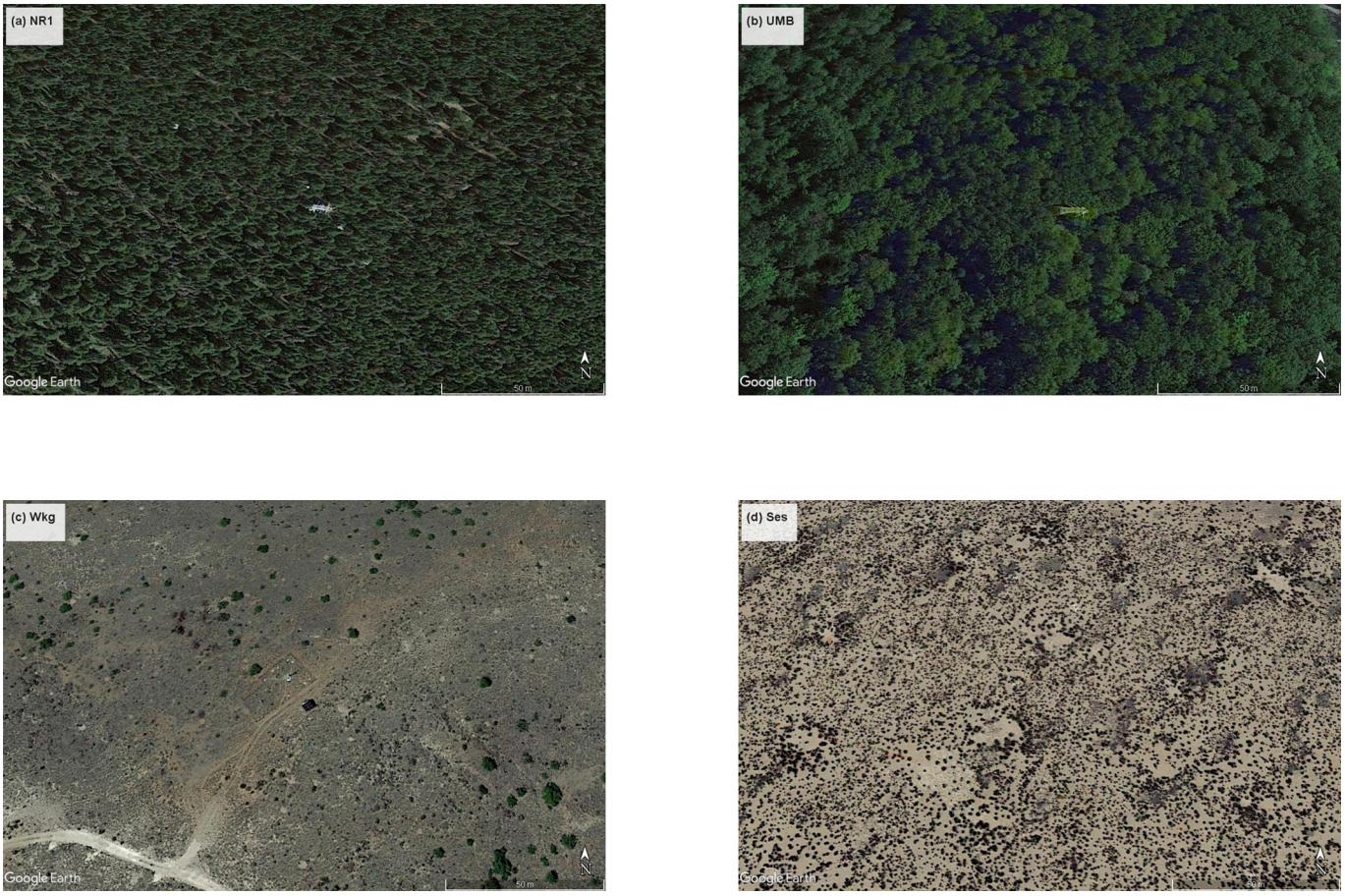

Fig. 6. High resolution images for the two forest sites and two desert grassland sites from Google Earth.

and winter, few of the standard deviations are above 2.5 K. During the night-time, the standard deviations are below 1.5 K in all the seasons. Thus, we propose that the correction for LST directionality is needed when the standard deviation of directional LST in the principal plane is above 2.5 K.

To account for the different magnitudes of SULR estimates for the daytime and night-time, the RRMSEs for different methods were calculated for summer when LST directionality is the strongest (Table 4). Consistent with the previous statistics, the improvement after correcting for LST directionality is negligible at night for both the MYD11 and MYD21 LST data as compared to that in the day. For the daytime, the improvement after correcting for LST directionality is much more notable for the MYD21 LST (1.6%) than for the MYD11 LST (0.5%), which is also in good agreement with the conclusion drawn based on RMSE and bias.

Overall, the proposed SULR estimation method in this study achieves good accuracy (Table 5). The RMSEs of SULR estimates using the MYD11 and MYD21 LST are both around 10 W m^{-2}, with the RMSE using MYD21 slightly lower. The absolute biases are within 5 W m^{-2} and the bias using the MYD21 LST is close to 0.

4.3. Spatial distributions of SULR estimates

SULR over the Iberian Peninsula and north Africa in summer was mapped to exemplify its spatial distribution and the correction effect of the proposed method (Fig. 9). Over the semiarid Iberian Peninsula, there is a large spatial variation in SULR, ranging from 400 to 650 W m^{-2}. After correcting for LST directionality, SULR was lowered in most regions due to the overestimation of SULR using the directional LST (c.f. Fig. 5(b)). Most of the SULR differences (Fig. 9(c)) are between 10 and 20 W m^{-2}, which is consistent with the accuracy improvement at the sites in semiarid regions in Figs. 4 and 5. The difference is larger (~20 W

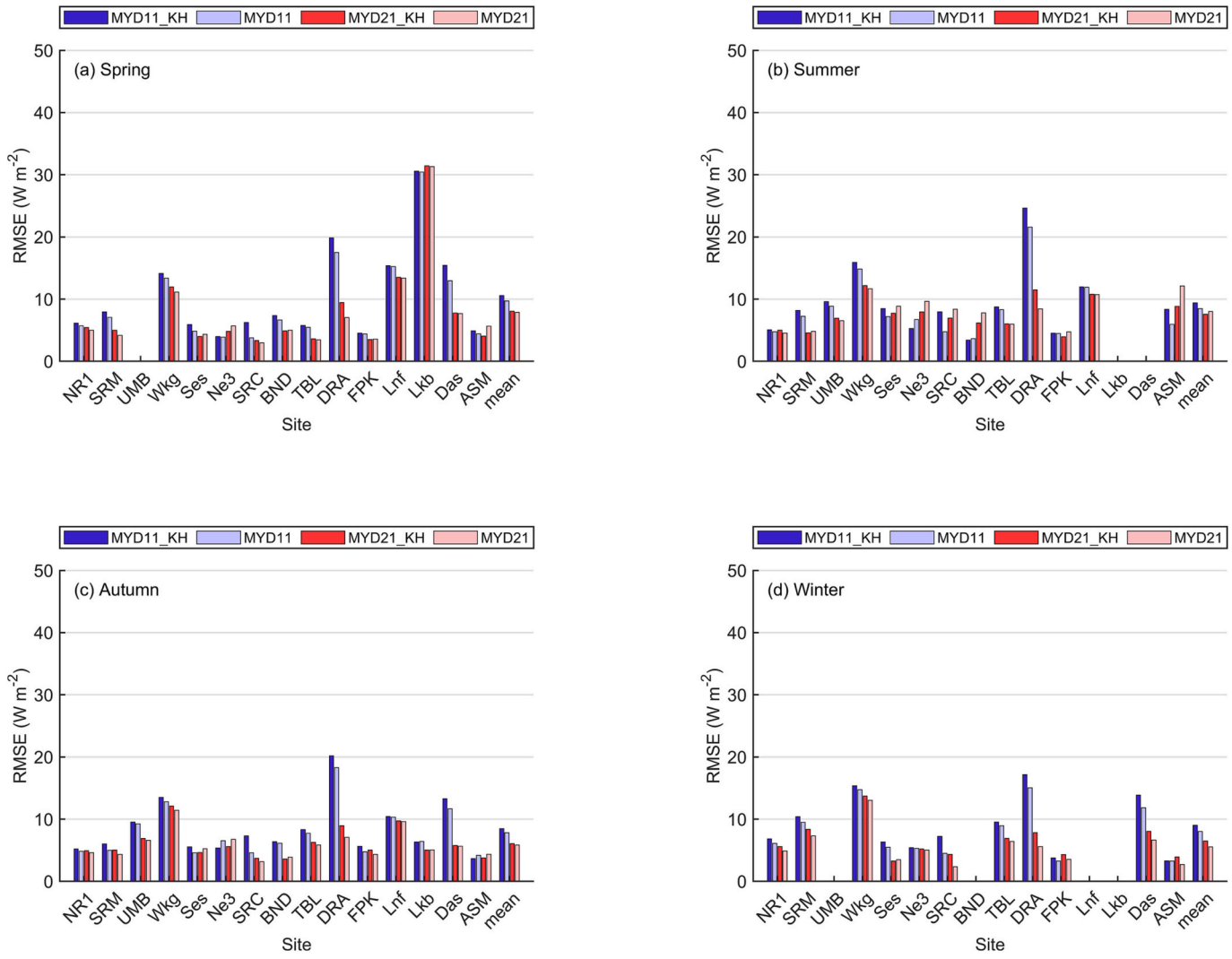

Fig. 7. RMSE of the SULR estimates in (a) spring, (b) summer, (c) autumn and (d) winter for the night-time.

m^{-2}) in the sparsely vegetated regions (eastern part of Iberian Peninsula). In contrast, the difference is below 10 W m^{-2} in the relatively more densely vegetated regions (western part). In these semiarid regions, both the hotspot kernel and emissivity kernel have significant effects on LST directionality due to the substantial shadowing effects over savannas and large proportions of soil over the land surface. Over the arid north Africa, the differences are generally higher, which are between 20 and 30 W m^{-2}, which is associated with the anisotropic effects of emissivity considering the relatively flat landscape in these regions. Overall, the difference between SULR estimates before and after correcting LST directionality is marked and consistent with the previous analyses at the ground sites. This confirms that significance of accounting for LST directionality in SULR estimation.

4.4. Equivalent viewing direction for SULR estimation

Results of KGE for all sites at different values of VZA in the back-scattering direction are shown in Fig. 10 considering the existence of such a surrogating angle in the back-scattering direction in the simulation (Figs. 2 and 3). Note that the dependence of KGE on VZA is very similar for estimates using either MYD11 or MYD21 LST, with a convex curve between 50° and 60°. In spring, KGE reaches a peak for VZA slightly above 54°. In summer, KGE also peaks at 54°, thus reaching the same value as in spring despite of different Sun paths. Thus, we advise to retain 54° at the back-scattering direction for the equivalent VZA.

The comparison between SULR estimates from hemispherical integration and from the directional LST estimated at the equivalent VZA angle in summer is shown in Figs. 11. The SULR estimates using the LST at 54° is quite consistent with those after correcting for LST directionality. The differences of bias and RMSE are generally within 3 W m^{-2} at most sites.

It is worth mentioning that the equivalent viewing angle for estimating SULR in this study is a local optimum angle for estimating SULR that approaches the hemispherical estimation rather than a global optimum angle. Detailed mathematical deductions are needed to investigate the possibility to find a global surrogating angle, which is out of the scope of this study.

5. Discussion

5.1. Influence of vegetation density on SULR estimates

Diurnal cycle and seasonal trend have a strong influence on LST directionality and therefore SULR estimates, which is modulated by different features of the land unit. To explore the impact of vegetation density, time series of leaf area index (LAI) and RMSE before and after correcting for LST directionality using the MYD21 LST at different sites are shown in Fig. 12. At the sites SRM, Ses, Wkg, SRC, DRA, Das, and ASM in the semiarid regions, LAI is almost constant throughout the year and remains around 0.1, which indicates a very sparse vegetation.

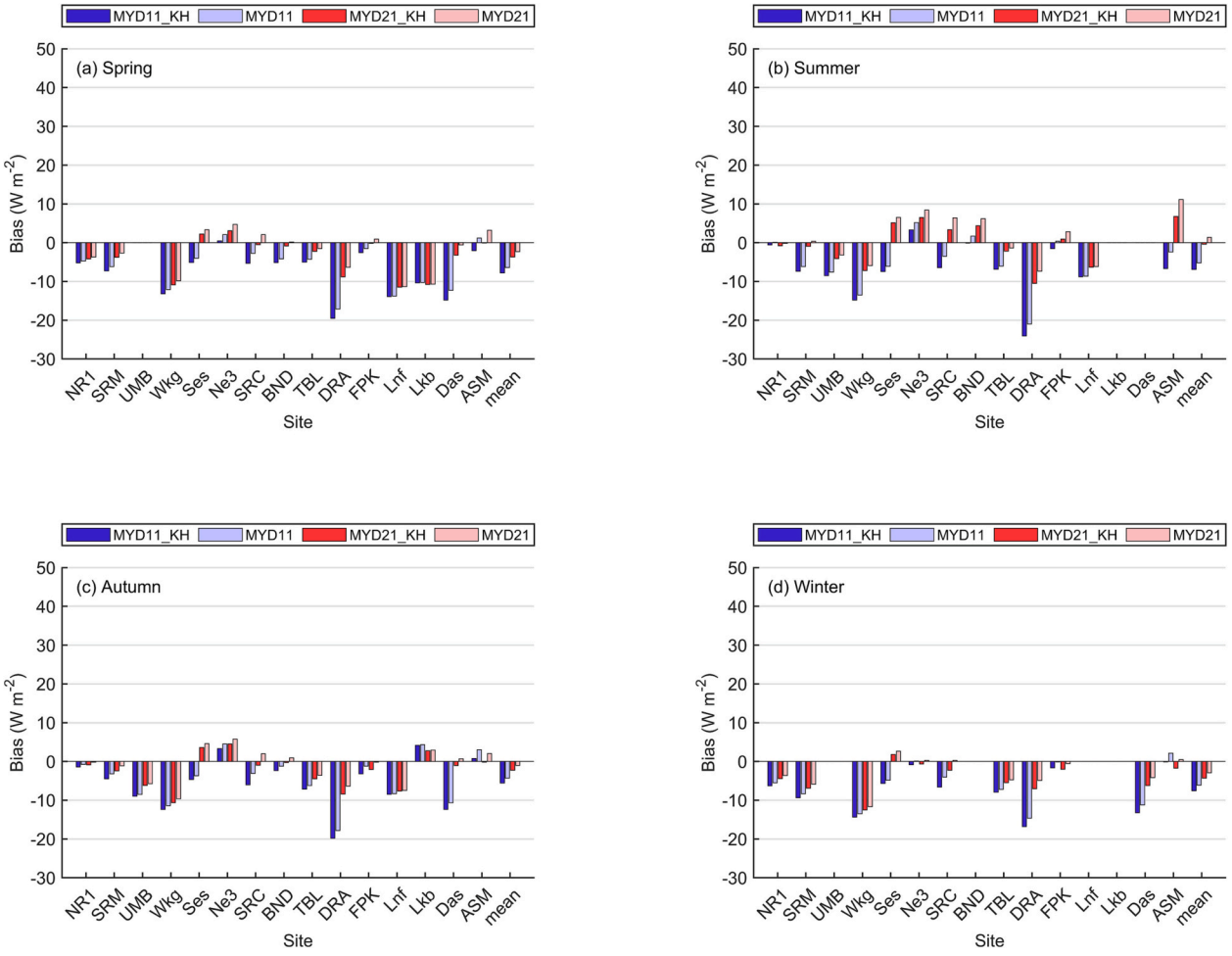

Fig. 8. Biases of the SULR estimates in (a) spring, (b) summer, (c) autumn and (d) winter for the night-time.

Table 4
RRMSE results of the four methods at different sites in summer. The cases with sample numbers below 20 are excluded.

Site	MYD11_KH		MYD11		MYD21_KH		MYD21	
	Day	Night	Day	Night	Day	Night	Day	Night
NR1	4.3%	1.4%	6.6%	1.4%	4.4%	1.4%	6.7%	1.3%
SRM	–	2.0%	–	1.8%	–	1.1%	–	1.2%
UMB	3.3%	2.5%	2.3%	2.3%	2.2%	1.8%	2.8%	1.7%
Wkg	3.2%	4.0%	4.9%	3.7%	4.4%	3.0%	6.1%	2.9%
Ses	1.7%	2.2%	2.5%	1.8%	4.2%	1.9%	6.0%	2.2%
Ne3	4.4%	1.3%	4.7%	1.7%	5.8%	2.0%	7.3%	2.4%
SRC	–	1.9%	–	1.1%	–	1.6%	–	2.0%
BND	4.1%	0.9%	3.5%	0.9%	3.1%	1.5%	4.8%	1.9%
TBL	3.4%	2.3%	3.8%	2.2%	2.7%	1.6%	4.3%	1.6%
DRA	–	6.2%	–	5.4%	–	2.8%	–	2.0%
FPK	2.4%	1.2%	2.6%	1.2%	2.1%	1.1%	3.5%	1.3%
Lnf	–	3.3%	–	3.2%	–	2.9%	–	2.9%
ASM	–	1.9%	–	1.4%	–	2.0%	–	2.7%
Mean	3.4%	2.4%	3.9%	2.2%	3.6%	1.9%	5.2%	2.0%

Table 5
Overall evaluation results using the proposed method. The SULR estimates were obtained by retaining the common ones retrieved from the four estimation methods after outlier removal.

Site	MYD11_KH		MYD21_KH	
	Bias	RMSE	Bias	RMSE
NR1	−1.44	7.16	−0.94	6.90
SRM	−4.99	8.21	−1.12	7.36
UMB	−7.94	12.32	−2.22	9.68
Wkg	−0.43	15.68	3.18	16.74
Ses	−4.51	6.54	6.00	8.94
Ne3	0.78	6.58	3.87	7.58
SRC	−5.39	6.88	1.20	5.53
BND	−3.81	8.55	1.26	7.42
TBL	−7.42	9.63	−3.59	6.93
DRA	−20.37	20.94	−8.06	9.33
FPK	−3.95	7.06	−0.81	6.38
Lnf	−7.21	11.95	−3.49	11.88
Lkb	1.05	10.71	2.84	9.72
Das	−3.56	13.63	7.25	17.12
ASM	0.76	5.37	2.67	6.36
Mean	−4.56	10.08	0.53	9.19

Remarkable improvements in SULR estimates are obtained after correcting LST directionality at these sparsely vegetated sites. This could be explained by the fact that the angular variation of narrow-band emissivity is significant over barren or sparsely vegetated surfaces (Hu et al., 2019b). This will enhance the angular effects in the LST retrieval process although surface heterogeneity is insignificant at these sites. Moreover, the impact of emissivity directionality on LST angular variation tends to be amplified at high temperatures (Trigo et al., 2021). For the other vegetated sites, LAI shows substantial seasonal variations. During summer, LAI at these vegetated sites (except at UMB) corresponds to medium vegetation coverage with significant shadowing effects. This is consistent with the significant improvement of SULR after correcting LST directionality. At the site UMB in summer, LAI value is beyond 4, which indicates a relatively dense canopy and therefore weak thermal

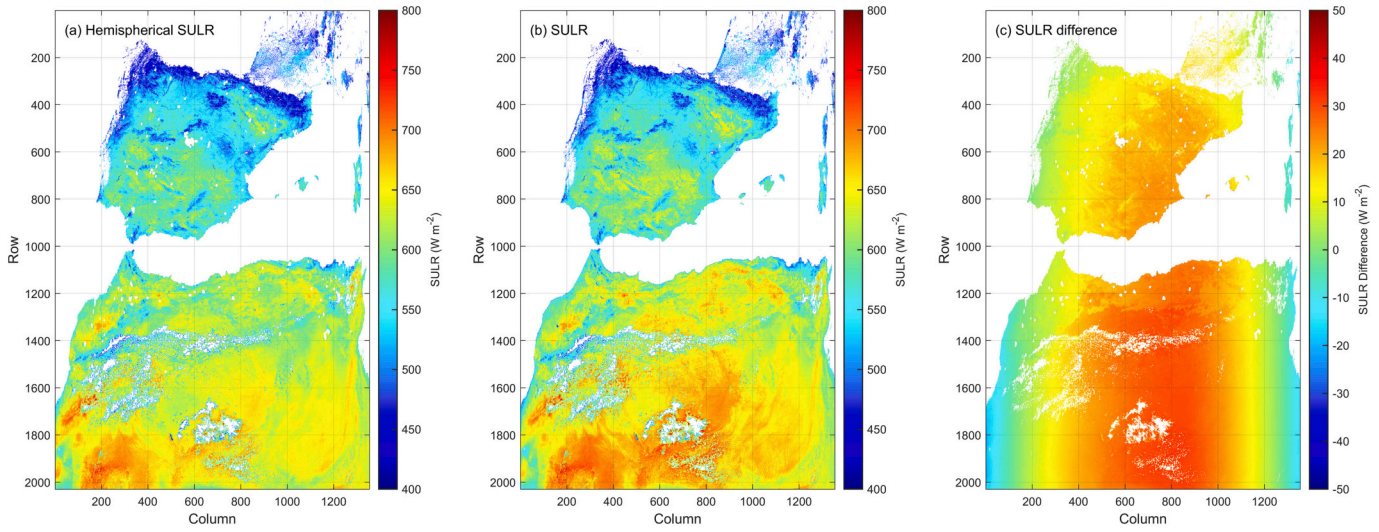

Fig. 9. SULR mapping over the Iberian Peninsula and north Africa on July 13, 2010. The overpass time (UTC) was 13:15. The LST and emissivity from the MYD21 swath data were used. DLR was obtained from the ERA5 data after bilinear interpolation. (a) and (b) are SULR estimates after and before correcting LST directionality, (c) is the difference ((b) minus (a)) between these two.

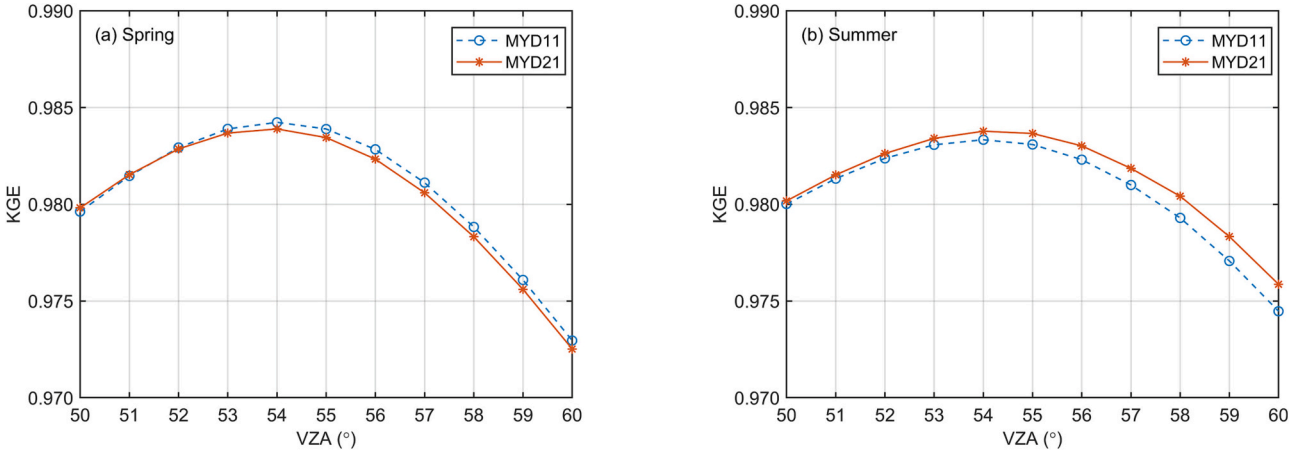

Fig. 10. KGE of SULR calculated using the directional LST at different VZA values for the daytime in (a) spring and (b) summer. The SULR obtained from hemispherical integral is regarded as the reference. Estimates at all sites are put together in the KGE calculation.

directionality. This agrees with the negligible change of SULR after correcting LST directionality at the site UMB in summer.

5.2. Influence of LST accuracy on SULR estimates

MYD11 and MYD21 LST data show contrasting performances in SULR estimation at the site DRA. For the daytime, the accuracy of SULR estimates using the MYD11 LST was obviously degraded after correcting LST directionality whereas that using the MYD21 LST was improved after correcting LST directionality. For the night-time, the SULR estimates using the MYD11 LST had much larger RMSEs and absolute biases than those using the MYD21 LST at DRA whereas the estimates using these two LST data were similar at the other sites. At Ses and Das, the accuracy of SULR estimates using the MYD11 LST was substantially higher than that using the MYD21 LST. At the other sites, the performances of these two LSTs were similar.

To investigate the difference between these two MODIS LST data, an evaluation was carried out based on the in-situ measurements (Fig. 13). Only the LST data with good quality as indicated in the quality flag were used. The outliers were removed using the same approach than in Section 3.3. The in-situ LST was estimated by inverting the Stefan-Boltzmann's law as follows:

$$T_s = \sqrt[4]{\frac{R_{up} - (1 - \varepsilon_{BB})R_{down}}{\varepsilon_{BB}\sigma}} \tag{12}$$

where R_{up} and R_{down} are the measured upward and downward longwave radiations, respectively, ε_{BB} is the broadband emissivity calculated using Eq. 5 and σ is the Stefan-Boltzmann constant.

For the sparsely vegetated site DRA, MYD21 LST shows a smaller RMSE and absolute bias (~2 K) compared to MYD11 LST, which is consistent with the higher accuracy of SULR estimates using the MYD21 LST compared to that using the MYD11 LST at DRA. An explanation could be that MYD21 LST uses a physical emissivity, which is more accurate than the classification-based emissivity used for MYD11 LST at the site DRA (Hu et al., 2019a; Li et al., 2021). The large underestimation of MYD11 LST tends to propagate to the entire upper hemisphere when the directional LST is calculated using the KDM. Therefore, the accuracy of SULR estimates after correcting LST directionality using the MYD11 LST at DRA is degraded, with a large negative bias between −15 and − 20 W m^{-2}.

At Ses and Das, the absolute bias and RMSE of the MYD 11 LST is ~1

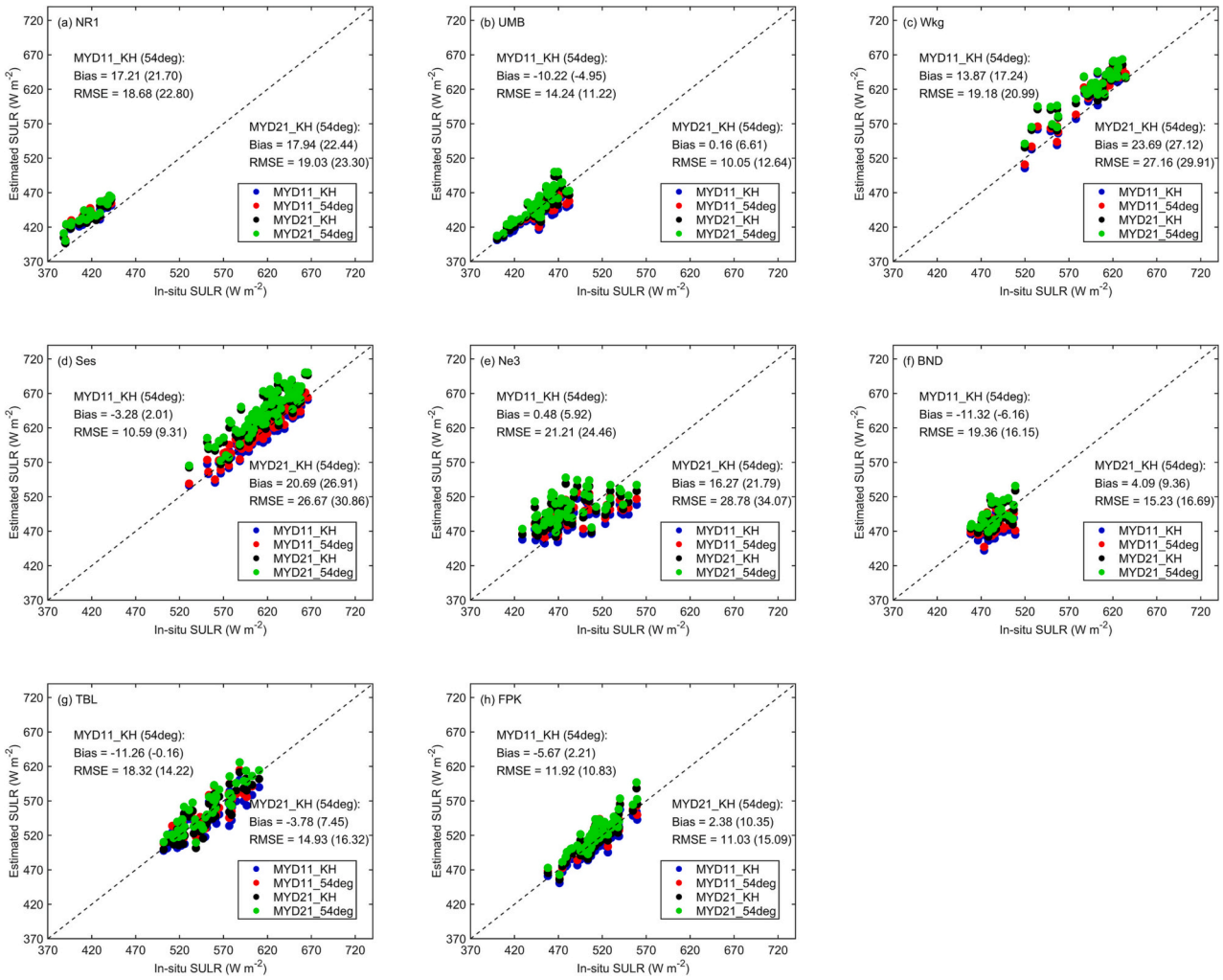

Fig. 11. Scatterplots of SULR estimates after correcting for LST directionality (MYD11_KH, MYD21_KH) and those using the 54° LST (MYD11_54deg, MYD21_54deg) in summer for the daytime. The cases with sample numbers <20 are excluded.

K smaller than those of the MYD21 LST. This agrees well with the higher accuracy of SULR estimates using the MYD 11 LST as compared to that using the MYD21 LST at the two sites. For the other sites, the accuracies of the two LST products are similar and consistent with their similar performances in SULR estimation.

5.3. *Influence of temporal variations in model coefficients on SULR estimates*

LST directionality is expected to have marked seasonal variation due to the variation in vegetation coverage and sun illumination throughout the year. Ermida et al. (2018b) analyzed the impact of such seasonality on the parametric models. It was reported that monthly calibration and annual calibration of the model coefficients did not impact the accuracy of the KDMs significantly (ΔRMSE <0.1 K) despite of the high variation in model parameters. This is because the temporal variability of LST directionality is to some extent incorporated in the KDM through nadir-viewing temperature, sun zenith angle and daily TOA radiation (Ermida et al., 2018b). Thus, the annually calibrated Kernel-Hotspot model is used in this study to allow for more samples with a wider range of illumination angles. Nevertheless, the emissivity kernel does not depend on the solar angle. Thus, the emissivity kernel does not suffer the sampling problem and a seasonal fit would be possible for the emissivity kernel in the future. This is expected to further improve the model performance over surfaces with substantial seasonal variations in vegetation coverage, thereby reducing uncertainties in SULR estimates.

The model coefficients calibrated in 2011 were used for both 2010 and 2011. To investigate the influence of inter-annual variation in retrieved model coefficients on SULR estimates, the accuracy of SULR was calculated separately for each year (Table 6). The decreases of average RMSE and absolute biases after correcting LST directionality are almost the same for each year, with the average RMSE and absolute bias approximately 5 and 6 W m^{-2} lower after correcting LST directionality. Therefore, we conclude that the extrapolation of model coefficients to 2010 does not significantly impact the performance of the Kernel-Hotspot model in SULR estimation. However, for years with a large gap from the calibration year, a recalibration of the model coefficients may be needed to guarantee the model accuracy.

5.4. *SULR estimated from nadir viewing LST*

For the sake of normalizing LST products, directional LST is normally corrected from oblique to nadir viewing (Ermida et al., 2018a). A comparison between the SULR estimated from a hemispherical integration and from nadir view of LST is performed. Since the impact of LST directionality on SULR estimation is weak in autumn and winter for the daytime and in all seasons for the night-time, only the results in spring and summer for the daytime are shown (Figs. 14 and 15). It is found that SULR estimates using nadir viewing LST have larger RMSE and absolute biases than those after correcting LST directionality in most cases.

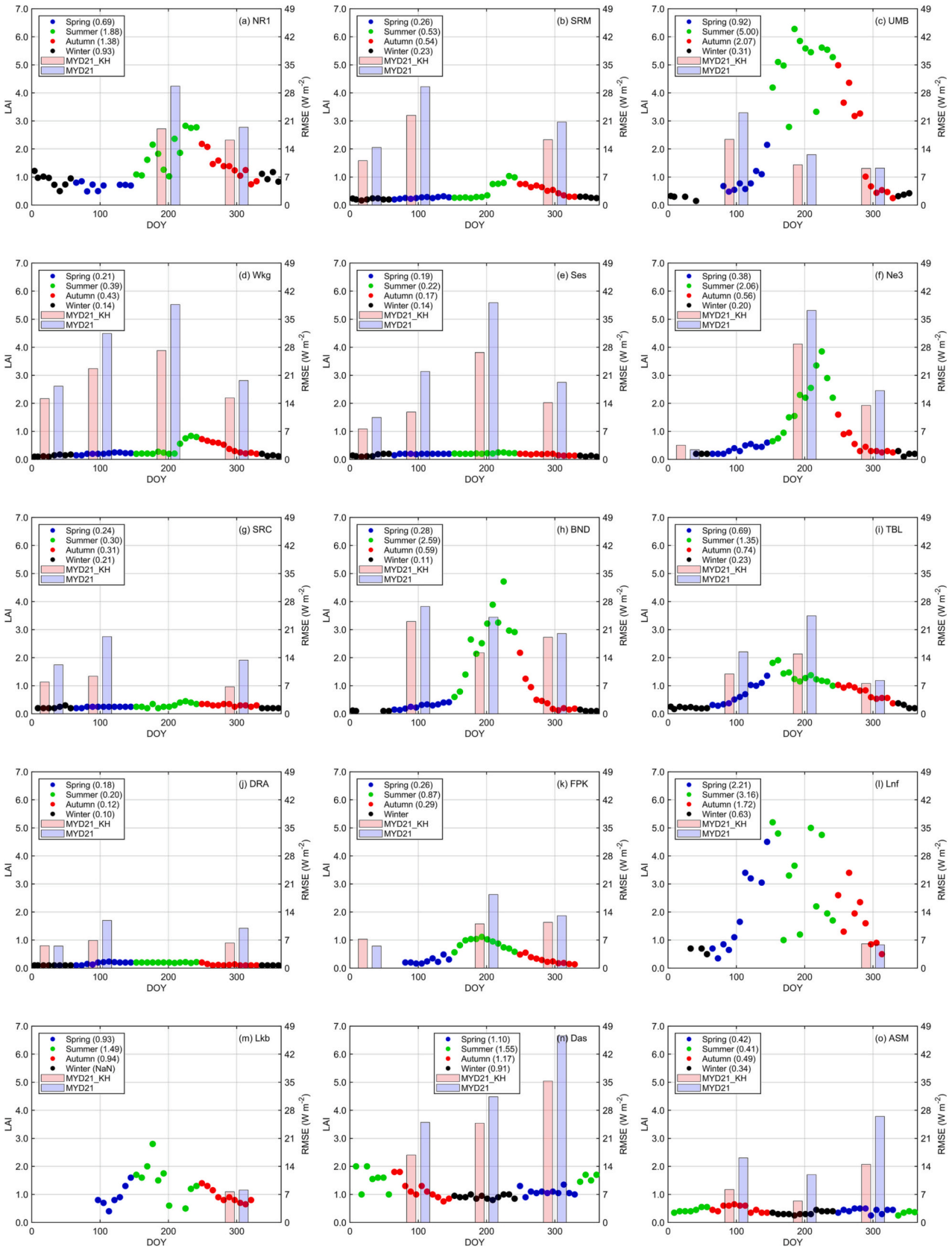

Fig. 12. Time series of LAI at different sites. The 8-day composited MYD15A2H LAI data in 2010 and 2011 were used. The LAI in a window of 2 × 2 containing each site were averaged to match the 1-km spatial resolution of LST data. The data for the same day-of-year (DOY) in the two years were averaged to represent the corresponding DOY. Only LAI of good quality was used. The RMSE of SULR was for the daytime and calculated using the MYD21 LST.

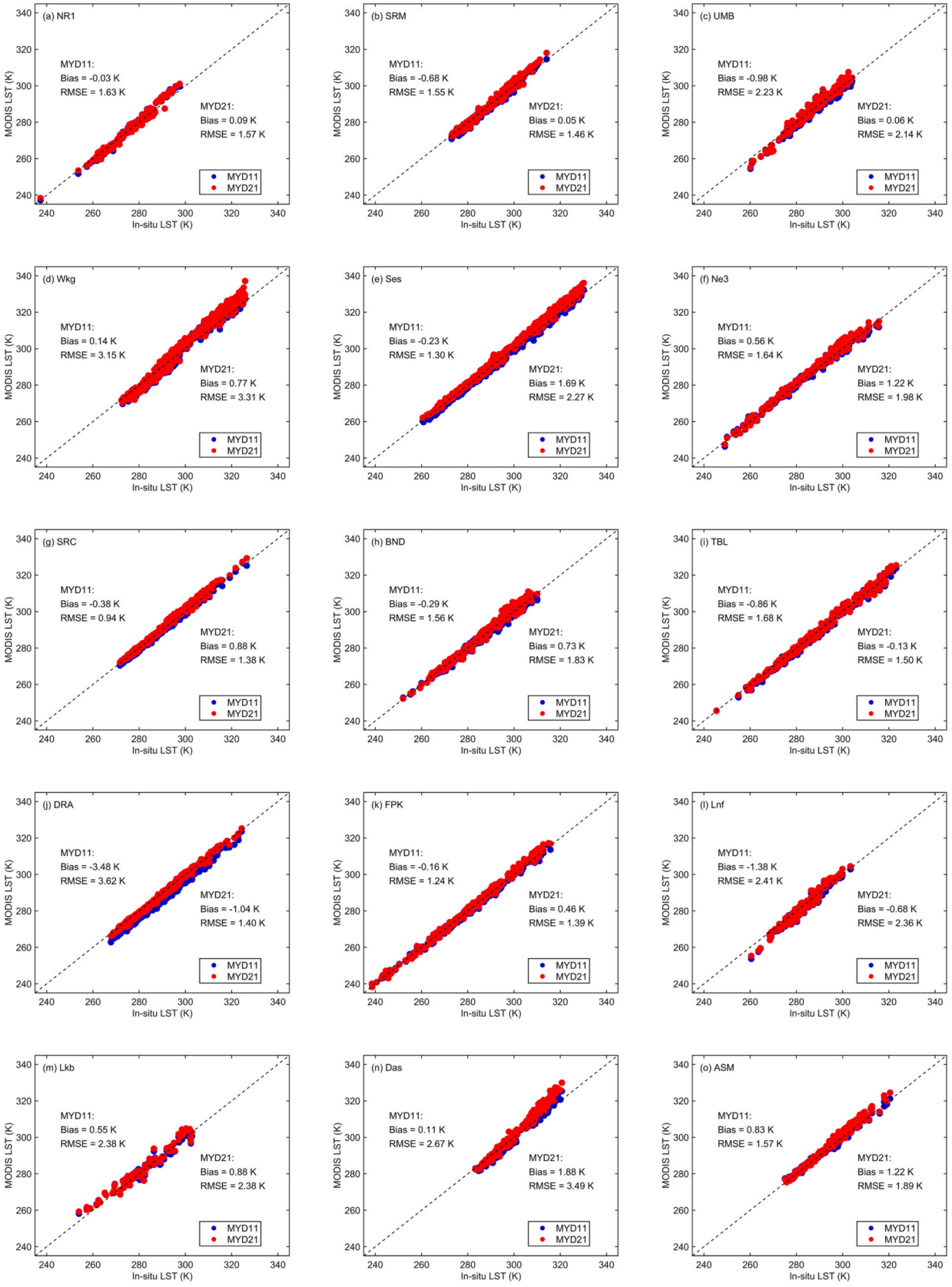

Fig. 13. Comparison of the MYD11 and MYD21 LST products with in-situ measurements for the period between 2010 and 2011.

Table 6
Comparison between results obtained using the MYD21_KH method at the SURFRAD sites in 2010 and 2011 for the daytime.

Site	Sample Number	MYD21_KH		MYD21		Sample Number	MYD21_KH		MYD21	
		Bias	RMSE	Bias	RMSE		Bias	RMSE	Bias	RMSE
	2010					2011				
NR1	29	16.49	17.96	20.98	22.30	19	16.57	17.47	26.26	27.43
SRM	63	13.71	15.62	17.34	20.55	65	14.89	20.13	19.40	25.38
UMB	56	3.08	9.76	8.06	13.39	41	2.77	9.99	7.21	11.77
Wkg	134	17.60	19.16	23.24	26.27	136	17.21	20.03	23.30	27.45
Ses	142	11.69	15.52	17.81	22.52	151	10.74	13.60	19.06	22.85
Ne3	60	5.20	27.91	13.06	31.09	66	5.99	13.83	13.00	21.64
SRC	64	5.11	7.67	11.32	13.55	56	6.49	8.57	13.15	15.63
BND	67	9.56	23.01	16.62	27.97	50	1.76	13.69	6.75	15.26
TBL	67	−1.68	9.91	5.57	15.38	71	−2.60	9.44	6.12	15.42
DRA	45	0.49	7.05	5.78	10.25	61	−1.71	5.88	4.15	9.02
FPK	68	1.74	10.25	7.11	13.51	75	1.70	11.49	8.02	14.79
Lnf	16	4.73	9.69	6.40	7.80	35	7.45	10.87	9.03	11.42
Lkb	11	0.01	11.36	2.88	12.49	23	−0.10	12.32	3.47	17.04
Das	60	30.68	32.95	38.80	41.57	81	14.25	17.36	21.55	25.27
ASM	22	13.50	16.23	24.29	26.40	91	5.37	7.47	12.12	15.11
Mean	–	8.79	15.60	14.62	20.34	–	6.72	12.81	12.84	18.37

Especially at the desert grassland sites (Wkg and Ses), the RMSEs when using the nadir LST are >25 W m^{-2} in spring and > 40 W m^{-2} in summer, increased by ~15 W m^{-2} in spring and ~ 20 W m^{-2} in summer as compared to those after correcting for LST directionality. At the sparsely vegetated sites SRC, Das, and ASM, the RMSE and bias of SULR using the nadir LST in spring are similarly increased substantially (~15 W m^{-2}). At the NR1 site, the accuracy of SULR estimates using the nadir viewing LST in summer is also remarkably degraded, with RMSE and absolute bias increased by >10 W m^{-2} in summer. For the other sites, the discrepancies are generally within 10 W m^{-2} in most cases. This is consistent with the conclusion by Otterman et al. (1995) that the hemispheric longwave radiation using a nadir measurement can produce large errors (~10%). In contrast, the accuracy of SULR estimates at DRA using the MYD11 LST is degraded in spring after correcting for LST directionality as compared to that using the nadir viewing LST (see Fig. 14h). This is consistent with the lower accuracy obtained after correcting LST directionality using the MYD11 LST at DRA in Figs. 4 and 5.

5.5. Site spatial representativeness

The 15 sites over different land surface types were selected carefully based on previous studies to ensure the spatial representativeness of the in-situ measurements at the MODIS pixel scale. To quantify the spatial homogeneity of the sites, we calculated the standard deviation of LST at each site using the high spatial resolution Landsat LST data (Fig. 16). Except for TBL, the medians of standard deviation at all the sites are below 1 K. The maximum standard deviations are below 1.5 K at all the sites except for BND, TBL, and Lkb. The good spatial homogeneity of the sites overall confirms the validity of the conclusions in this study.

5.6. Uncertainties and limitations

In the calculation of SULR, DLR was directly obtained from the in-situ measurements rather than from external datasets. This is to avoid the influence of uncertainties in DLR estimates on the analysis of LST directionality impacts although the influence is negligible due to the scaling factor 1 - ε.

Uncertainty may be introduced into the estimated directional LST from the Kernel-Hotspot model, thus impacting the SULR calculation. Cao et al. (2021) evaluated eight state-of-the-art KDMs using both simulation and airborne measured multi-angular data. The 4-stream radiative transfer model based on the Scattering by Arbitrarily Inclined Leaves (4SAIL) and the Discrete Anisotropic Radiative Transfer (DART) model were used to mimic the continuous canopy and discrete forest scene, respectively. For the airborne multi-angular data, two different datasets were used: one over continuous maize canopy collected in the northwestern China during the Watershed Allied Telemetry Experimental Research (WATER) experiment campaign and the other one over discrete pine canopy in Bordeaux, France. The evaluation results revealed that the RMSE values of the Kernel-Hotspot model were below 0.2 K in all cases using the simulation data. For the evaluation using the airborne dataset, the RMSE values of the Kernel-Hotspot model are ~0.2 K for both continuous and discrete scenes. Assuming the condition with a temperature of 300 K and a broadband emissivity of 0.96, the uncertainty caused in SULR by the modeling error of 0.2 K is approximately 1 W m^{-2}. Thus, the uncertainty introduced by the Kernel-Hotspot model into SULR estimation is negligible.

The Kernel-Hotspot model has a simple yet effective emissivity kernel, which dominates the LST directionality over areas where the shadowing/sunlit effects are minor and surface spatial heterogeneity is low (e.g., barren or sparsely vegetated surfaces). In the evaluation conducted by Ermida et al. (2018b), the RMSE of the KDM was between 0.1 and 0.2 K when the percentage of tree cover (PTC) was below 20% that indicates a sparsely vegetated surface. Especially at night when the emissivity directionality is the only factor contributing to LST directionality, the RMSEs of the KDM were below 0.2 K for all PTC cases. The good accuracy of the emissivity kernel was further confirmed by Cao et al. (2021). In their evaluation using simulations based on the 4SAIL and DART models, the RMSEs for the KDM were below 0.2 K for both scenarios (i.e., over continuous and discrete canopies) when LAI was set to 1. Further improvement of the emissivity kernel can be made possibly by considering the Hapke soil model for the simulation of soil emissivity directionality (Ermida et al., 2018b).

In the calibration of the KDM model coefficients, the SEVIRI LST and MODIS LST were used conjointly. The systematic differences between the two LST products were removed using a linear regression method based on MODIS LST (Ermida et al., 2017; Ermida et al., 2018a). Discrepancies may still occur after this exercise due to difference in footprint, not fully corrected from resampling, in surface orography, also in emissivity. The retrieved model coefficients could be in error, thereby impacting the SULR estimates. Moreover, the KDM model coefficients are in grids of 0.05° to coordinate the different pixel scales of SEVIRI (3 km), MODIS (1 km) LST and the other ancillary datasets used for extrapolating the model coefficients. Uncertainties can be introduced into SULR estimates when the model is applied to the MODIS 1 km LST product over heterogeneous surfaces. Despite of the aforementioned potential uncertainties in the KDM model calibration, the accuracy of SULR estimates after correction for LST directionality is still improved consistently at the selected sites. Thus, we conclude that the calibrated

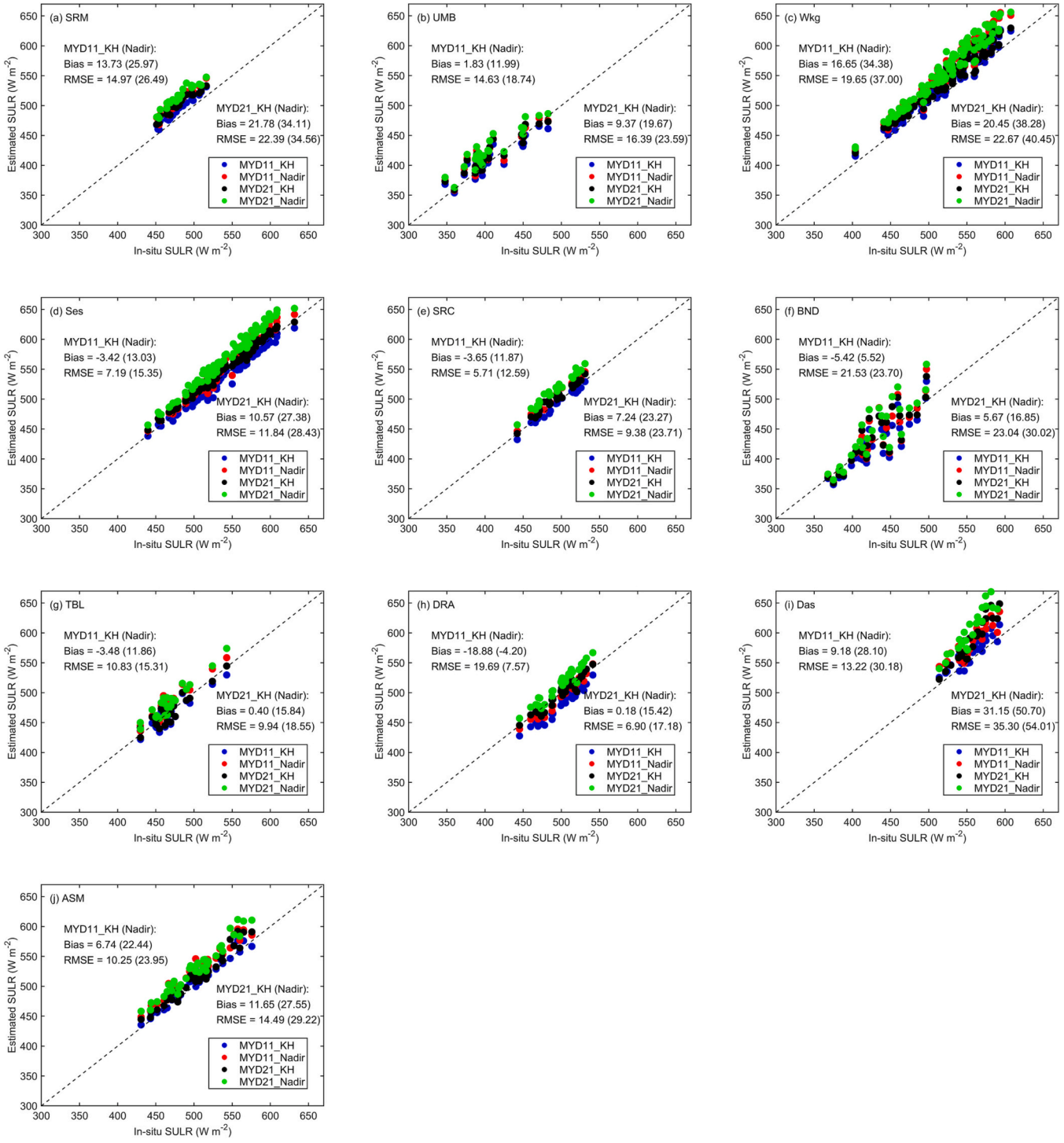

Fig. 14. Scatterplots of SULR estimates after correcting LST directionality and those using the nadir viewing LST in spring. The cases with sample numbers <20 are excluded.

Kernel-Hotspot model is effective in correcting for LST directionality in SULR estimation.

Since slope effects are not considered in the Kernel-Hotspot model, the proposed framework is probably not applicable over rugged surfaces. More information regarding the correction of thermal directionality in SULR estimation over high-relief terrain can be found in the studies by (Yan et al., 2020; Yan et al., 2016).

In the procedure of evaluation, the overfitting problem noticed in autumn and winter over most of the selected sites is due to the weak directional variation of LST. The consequence is a degradation of SULR accuracy after LST directionality correction. Therefore, we suggest that LST angular variation does not need to be considered in the SULR estimation when thermal directionality is minor, i.e., during autumn and winter for the daytime (except for in arid and semiarid regions) and in all seasons for the night-time.

6. Concluding remarks and perspectives

The angular variation in LST influences SULR estimation considering the significant thermal directionality of the land surface at the pixel

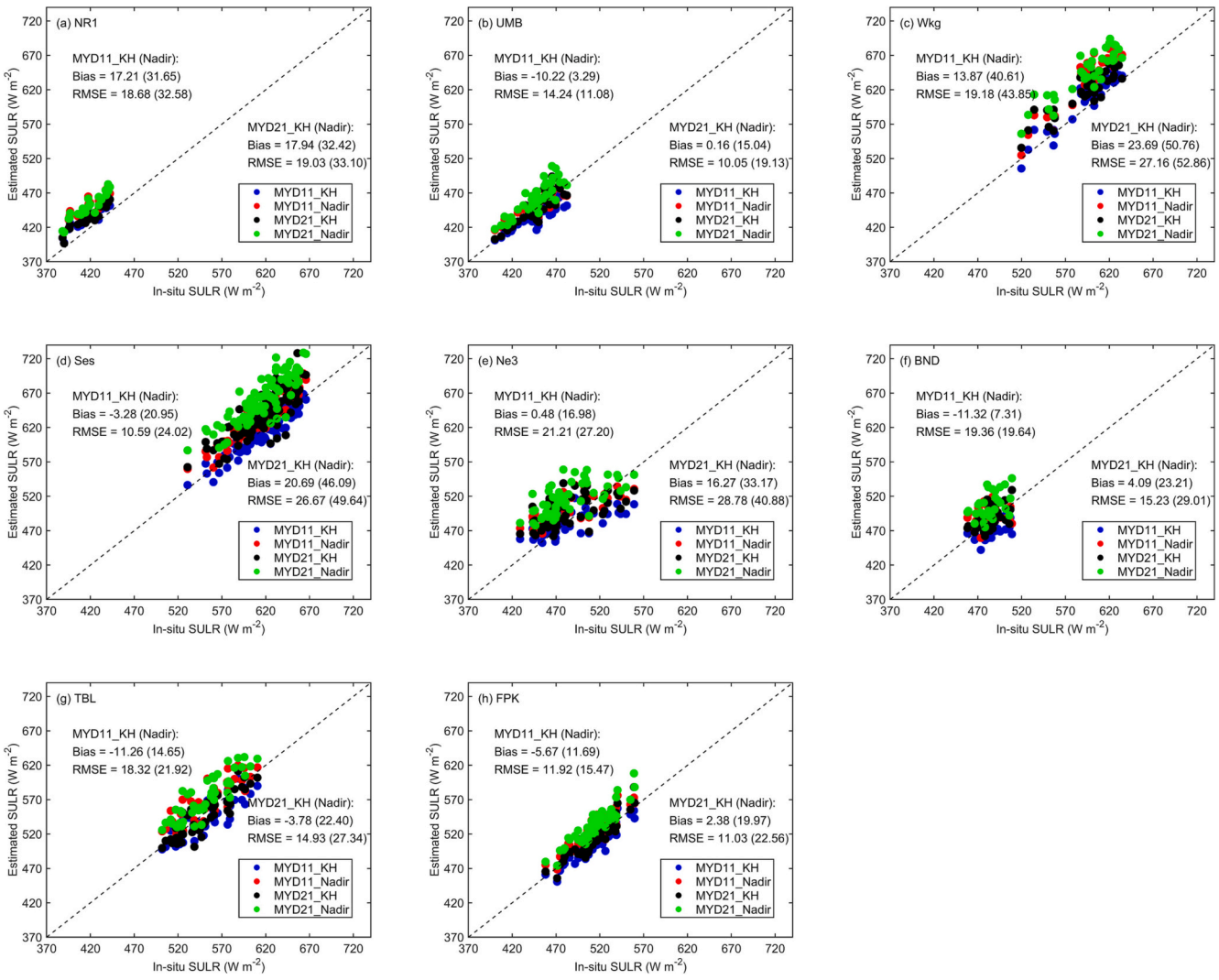

Fig. 15. Scatterplots of SULR estimates after correcting LST directionality and those using the nadir viewing LST in summer. The cases with sample numbers <20 are excluded.

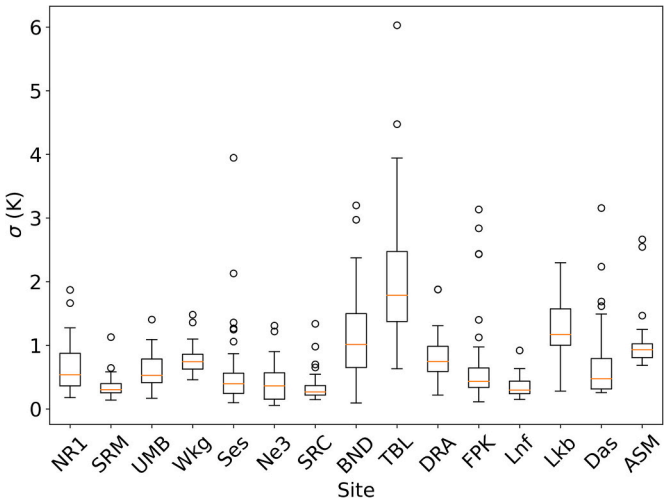

Fig. 16. Standard deviation of Landsat-8 LST in a window of 1 km × 1 km centred at each site. All the cloud-free Landsat images between 2015 and 2016 were used in the statistics.

scale. By incorporating a parametric model of LST directionality in the physical temperature-emissivity method, the present study analyzes the influence of LST directionality on SULR estimation using the MYD11 and MYD21 LST products. Evaluating the SULR estimates with respect to in-situ measurements from 15 different sites in different regions leads to the following conclusions.

LST directionality effects on SULR estimation exhibit diurnal and seasonal variations, which is conspicuous during spring and summer for the daytime. The effects are insignificant in autumn and winter for the daytime except for in arid and semiarid regions. For the night-time, the effects are insignificant over all the biomes. This behavior is consistent with the temporal variation of surface thermal directionality over different biomes.

Apart from the impacts of diurnal cycle and seasonal variation caused by solar illumination, the land unit is also associated with LST directionality effects on SULR estimation. This is reflected in the LST directionality model through the combination of the hotspot kernel depicting the shadowing effect and the emissivity kernel describing the emissivity directionality effect on LST.

The nadir viewing LST produces highly overestimated SULR and is therefore not the advised option for SULR estimation. The directional LST with VZA of 54° at the backward scattering direction can be regarded as a local optimum candidate for SULR estimation.

Despite the present analysis is conducted based on the MODIS LST

products and the Kernel-Hotspot LST anisotropy model, it is likely that this study could be extended to other LST products and models. Considering the simplicity and effectiveness demonstrated at the selected sites in different biomes, the developed SULR estimation model is promising to be integrated into surface energy balance models to improve the accuracy of ET retrieval over vegetated surfaces. This will facilitate the future thermal missions with respect to monitoring water use and water stress in the terrestrial ecosystems.

Future work will focus on generating SULR products using the developed model at large spatial scales for a long time series and evaluating the model performance extensively using in-situ measurements in various regions over the globe to further demonstrate the generality of the conclusions drawn from the selected 15 sites.

CRediT authorship contribution statement

Tian Hu: Conceptualization, Methodology, Software, Formal analysis, Writing – original draft, Writing – review & editing. **Jean-Louis Roujean:** Formal analysis, Writing – review & editing. **Biao Cao:** Formal analysis, Writing – review & editing. **Kaniska Mallick:** Formal analysis, Writing – review & editing. **Gilles Boulet:** Writing – review & editing. **Hua Li:** Writing – review & editing. **Zhihong Xu:** Writing – review & editing. **Yongming Du:** Writing – review & editing. **Qinhuo Liu:** Writing – review & editing.

Declaration of Competing Interest

The authors declare that they have no known competing financial interests or personal relationships that could have appeared to influence the work reported in this paper.

Data availability

Data will be made available on request.

Acknowledgement

This study was supported in part by the Natural Science Foundation of China under Grant 41930111, 42071317, 41871258 and in part by the Open Fund of State Key Laboratory of Remote Sensing Science of China (Grant No. OFSLRSS201903). Tian Hu and Kaniska Mallick also acknowledge the support of Luxembourg Institute of Science and Technology. The authors wish to extend their gratitude to Dr. Sofia L. Ermida and Dr. Isabel F. Trigo, who provided the global map of calibrated model coefficients and assistance in the model interpretation.

Appendix A

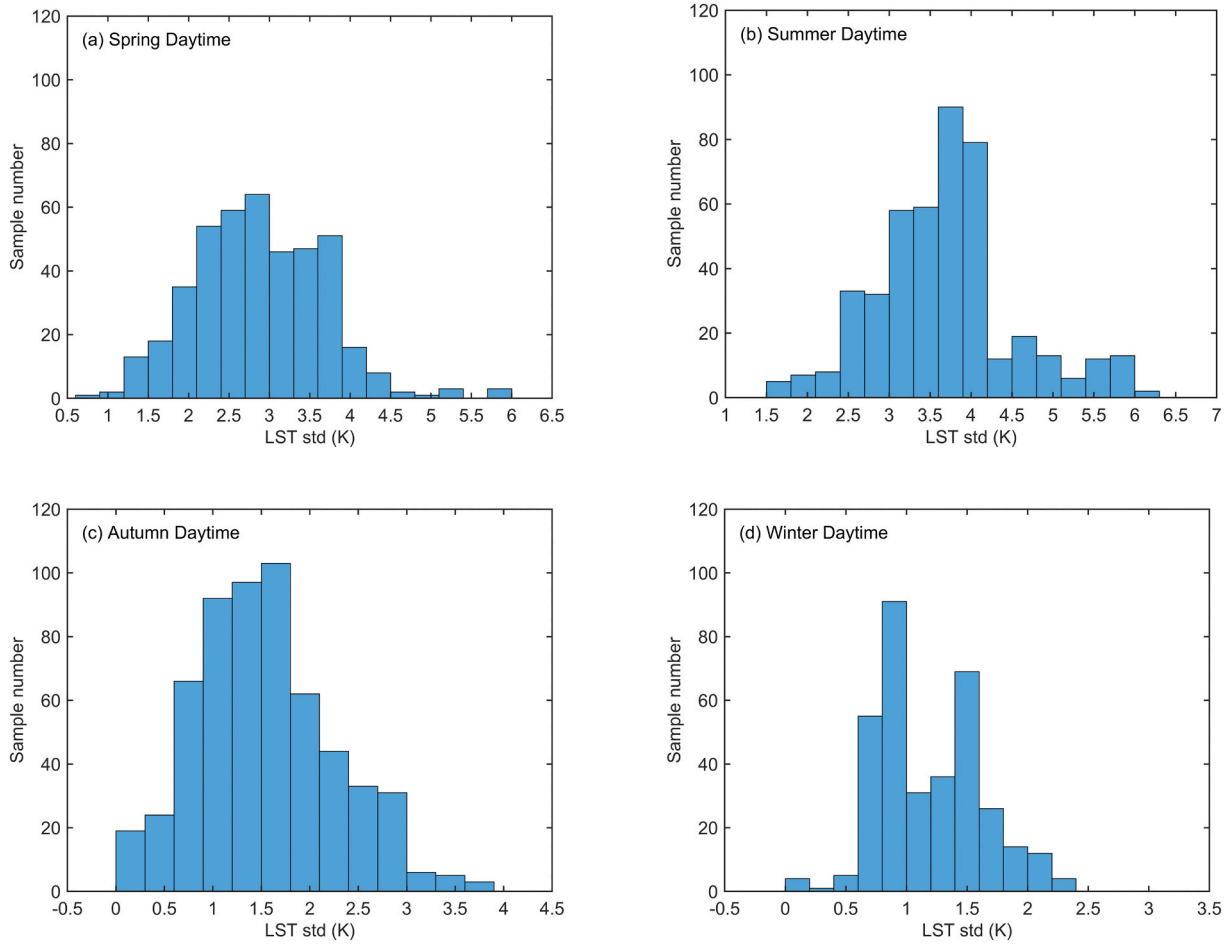

Fig. A1. Histograms of standard deviation of directional LST in the principal plane combining all the sites in (a) spring, (b) summer, (c) autumn, and (d) winter for the daytime

References

Anderson, M.C., Norman, J.M., Mecikalski, J.R., Otkin, J.A., Kustas, W.P., 2007. A climatological study of evapotranspiration and moisture stress across the continental United States based on thermal remote sensing: 1. Model formulation. J. Geophys.Res.Atmos. 112.

Bian, Z., Roujean, J.L., Lagouarde, J.P., Cao, B., Li, H., Du, Y., Liu, Q., Xiao, Q., Liu, Q., 2020. A semi-empirical approach for modeling the vegetation thermal infrared directional anisotropy of canopies based on using vegetation indices. ISPRS J. Photogramm. Remote Sens. 160, 136–148.

Cao, B., Gastellu-Etchegorry, J.-P., Du, Y., Li, H., Bian, Z., Hu, T., Fan, W., Xiao, Q., Liu, Q., 2019a. Evaluation of four kernel-driven models in the thermal infrared band. IEEE Trans. Geosci. Remote Sens. 57, 5456–5475.

Cao, B., Liu, Q., Du, Y., Roujean, J.-L., Gastellu-Etchegorry, J.-P., Trigo, I.F., Zhan, W., Yu, Y., Cheng, J., Jacob, F., Lagouarde, J.-P., Bian, Z., Li, H., Hu, T., Xiao, Q., 2019b. A review of earth surface thermal radiation directionality observing and modeling: historical development, current status and perspectives. Remote Sens. Environ. 232, 111304.

Cao, B., Roujean, J.-L., Gastellu-Etchegorry, J.-P., Liu, Q., Du, Y., Lagouarde, J.-P., Huang, H., Li, H., Bian, Z., Hu, T., 2021. A general framework of kernel-driven modeling in the thermal infrared domain. Remote Sens. Environ. 252, 112157.

Cheng, J., Liang, S., 2014. Effects of thermal-infrared emissivity directionality on surface broadband emissivity and longwave net radiation estimation. IEEE Geosci.Remote Sens.Lett. 11, 499–503.

Cheng, J., Liang, S., 2016. Global estimates for high-spatial-resolution clear-sky land surface upwelling longwave radiation from MODIS data. IEEE Trans. Geosci. Remote Sens. 54, 4115–4129.

Cheng, J., Liang, S., Wang, W., Guo, Y., 2017. An efficient hybrid method for estimating clear-sky surface downward longwave radiation from MODIS data. J.Geophys.Res. Atmos. 122, 2616–2630.

Coll, C., Galve, J.M., Niclòs, R., Valor, E., Barberà, M.J., 2019. Angular variations of brightness surface temperatures derived from dual-view measurements of the advanced along-track scanning radiometer using a new single band atmospheric correction method. Remote Sens. Environ. 223, 274–290.

Davies, L., Gather, U., 1993. The identification of multiple outliers. J. Am. Stat. Assoc. 88, 782–792.

Duan, S.-B., Li, Z.-L., Li, H., Göttsche, F.-M., Wu, H., Zhao, W., Leng, P., Zhang, X., Coll, C., 2019. Validation of collection 6 MODIS land surface temperature product using in situ measurements. Remote Sens. Environ. 225, 16–29.

Duffour, C., Lagouarde, J.P., Roujean, J.L., 2016. A two parameter model to simulate thermal infrared directional effects for remote sensing applications. Remote Sens. Environ. 186, 250–261.

Ellingson, R.G., 1995. Surface longwave fluxes from satellite observations: a critical review. Remote Sens. Environ. 51, 89–97.

Ermida, S.L., DaCamara, C.C., Trigo, I.F., Pires, A.C., Ghent, D., Remedios, J., 2017. Modelling directional effects on remotely sensed land surface temperature. Remote Sens. Environ. 190, 56–69.

Ermida, S.L., Trigo, I.F., DaCamara, C.C., Pires, A.C., 2018a. A methodology to simulate LST directional effects based on parametric models and landscape properties. Remote Sens. 10, 1114.

Ermida, S.L., Trigo, I.F., DaCamara, C.C., Roujean, J.-L., 2018b. Assessing the potential of parametric models to correct directional effects on local to global remotely sensed LST. Remote Sens. Environ. 209, 410–422.

Gillespie, A., Rokugawa, S., Matsunaga, T., Cothern, J.S., Hook, S., Kahle, A.B., 1998. A temperature and emissivity separation algorithm for advanced spaceborne thermal emission and reflection radiometer (ASTER) images. IEEE Trans. Geosci. Remote Sens. 36, 1113–1126.

Göttsche, F.-M., Olesen, F.-S., Bork-Unkelbach, A., 2013. Validation of land surface temperature derived from MSG/SEVIRI with in situ measurements at gobabeb, Namibia. Int. J. Remote Sens. 34, 3069–3083.

Guillevic, P., Göttsche, F., Nickeson, J., Hulley, G., Ghent, D., Yu, Y., Trigo, I., Hook, S., Sobrino, J.A., Remedios, J., Román, M., Camacho, F., 2018. Land surface temperature product validation best practice protocol. In: Guillevic, P., Göttsche, F., Nickeson, J., Román, M. (Eds.), Good Practices for Satellite-Derived Land Product Validation. Land Product Validation Subgroup (WGCV/CEOS).

Gupta, H.V., Kling, H., Yilmaz, K.K., Martinez, G.F., 2009. Decomposition of the mean squared error and NSE performance criteria: implications for improving hydrological modelling. J. Hydrol. 377, 80–91.

Gupta, S.K., Kratz, D.P., Wilber, A.C., Nguyen, L.C., 2004. Validation of parameterized algorithms used to derive TRMM–CERES surface radiative fluxes. J. Atmos. Ocean. Technol. 21, 742–752.

Hoffmann, H., Nieto, H., Jensen, R., Guzinski, R., Zarco-Tejada, P., Friborg, T., 2016. Estimating evaporation with thermal UAV data and two-source energy balance models. Hydrol. Earth Syst. Sci. 20, 697–713.

Hu, T., Cao, B., Du, Y., Li, H., Wang, C., Bian, Z., Sun, D., Liu, Q., 2017. Estimation of surface upward longwave radiation using a direct physical algorithm. IEEE Trans. Geosci. Remote Sens. 55, 4412–4426.

Hu, T., Du, Y., Cao, B., Li, H., Bian, Z., Sun, D., Liu, Q., 2016. Estimation of upward longwave radiation from vegetated surfaces considering thermal directionality. IEEE Trans. Geosci. Remote Sens. 54, 6644–6658.

Hu, T., Li, H., Cao, B., van Dijk, A.I.J.M., Renzullo, L.J., Xu, Z., Zhou, J., Du, Y., Liu, Q., 2019a. Influence of emissivity angular variation on land surface temperature retrieved using the generalized split-window algorithm. Int. J. Appl. Earth Obs. Geoinf. 82, 101917.

Hu, T., Renzullo, L.J., Cao, B., van Dijk, A.I.J.M., Du, Y., Li, H., Cheng, J., Xu, Z., Zhou, J., Liu, Q., 2019b. Directional variation in surface emissivity inferred from the MYD21 product and its influence on estimated surface upwelling longwave radiation. Remote Sens. Environ. 228, 45–60.

Hu, T., Renzullo, L.J., van Dijk, A.I.J.M., He, J., Tian, S., Xu, Z., Zhou, J., Liu, T., Liu, Q., 2020a. Monitoring agricultural drought in Australia using MTSAT-2 land surface temperature retrievals. Remote Sens. Environ. 236, 111419.

Hu, T., van Dijk, A.I.J.M., Renzullo, L.J., Xu, Z., He, J., Tian, S., Zhou, J., Li, H., 2020b. On agricultural drought monitoring in Australia using Himawari-8 geostationary thermal infrared observations. Int. J. Appl. Earth Obs. Geoinf. 91, 102153.

Hulley, G., Malakar, N., Hughes, T., Islam, T., Hook, S., 2016. Moderate Resolution Imaging Spectroradiometer (MODIS) MOD21 Land Surface Temperature and Emissivity Algorithm Theoretical Basis Document. Jet Propulsion Laboratory, NASA, Pasadena, CA.

Jiao, Z., Yan, G., Zhao, J., Wang, T., Chen, L., 2015. Estimation of surface upward longwave radiation from MODIS and VIIRS clear-sky data in the Tibetan plateau. Remote Sens. Environ. 162, 221–237.

Lagouarde, J.P., Irvine, M., 2008. Directional anisotropy in thermal infrared measurements over Toulouse city Centre during the CAPITOUL measurement campaigns: first results. Meteorog. Atmos. Phys. 102, 173.

Li, H., Li, R., Yang, Y., Cao, B., Du, Y., Bian, Z., Hu, T., Sun, L., Liu, Q., 2021. Temperature-based and radiance-based validation of the collection 6 MYD11 and MYD21 land surface temperature products over barren surfaces in northwestern China. IEEE Trans. Geosci. Remote Sens. 59, 1794–1807.

Li, H., Sun, D., Yu, Y., Wang, H., Liu, Y., Liu, Q., Du, Y., Wang, H., Cao, B., 2014. Evaluation of the VIIRS and MODIS LST products in an arid area of Northwest China. Remote Sens. Environ. 142, 111–121.

Li, H., Yang, Y., Li, R., Wang, H., Cao, B., Bian, Z., Hu, T., Du, Y., Sun, L., Liu, Q., 2019. Comparison of the MuSyQ and MODIS collection 6 land surface temperature products over barren surfaces in the Heihe River basin, China. IEEE Trans. Geosci. Remote Sens. 57, 8081–8094.

Liang, S., Wang, D., He, T., Yu, Y., 2019. Remote sensing of earth's energy budget: synthesis and review. Int.J.Digital Earth 12, 737–780.

Liang, S., Wang, K., Zhang, X., Wild, M., 2010. Review on estimation of land surface radiation and energy budgets from ground measurement, remote sensing and model simulations. IEEE J.Select.Top.Appl.Earth Observ.Remote Sens. 3, 225–240.

Liang, S., Cheng, J., Jia, K., Jiang, B., Liu, Q., Xiao, Z., Yao, Y., Yuan, W., Zhang, X., Zhao, X., 2021. The global land surface satellite (GLASS) product suite. Bull. Am. Meteorol. Soc. 102, E323–E337.

Mallick, K., Toivonen, E., Trebs, I., Boegh, E., Cleverly, J., Eamus, D., Koivusalo, H., Drewry, D., Arndt, S.K., Griebel, A., 2018. Bridging thermal infrared sensing and physically-based evapotranspiration modeling: from theoretical implementation to validation across an aridity gradient in Australian ecosystems. Water Resour. Res. 54, 3409–3435.

Mallick, K., Trebs, I., Boegh, E., Giustarini, L., Schlerf, M., Drewry, D.T., Hoffmann, L., Randow, C.V., Kruijt, B., Araùjo, A., 2016. Canopy-scale biophysical controls of transpiration and evaporation in the Amazon Basin. Hydrol.Earth Syst.Sci. 20, 4237–4264.

Meeus, J.H., 1991. Astronomical algorithms, 2 nd ed. Willmann-Bell, Incorporated, Richmond, VA, USA.

Otterman, J., Susskind, J., Brakke, T., Kimes, D., Pielke, R., Lee, T.J., 1995. Inferring the thermal-infrared hemispheric emission from a sparsely-vegetated surface by directional measurements. Bound.-Layer Meteorol. 74, 163–180.

Qin, B., Cao, B., Li, H., Bian, Z., Hu, T., Du, Y., Yang, Y., Xiao, Q., Liu, Q., 2020. Evaluation of six high-spatial resolution clear-sky surface upward longwave radiation estimation methods with MODIS. Remote Sens. 12, 1834.

Rasmussen, M.O., Gottsche, F.-M., Olesen, F.-S., Sandholt, I., 2011. Directional effects on land surface temperature estimation from meteosat second generation for savanna landscapes. IEEE Trans. Geosci. Remote Sens. 49, 4458–4468.

Rasmussen, M.O., Pinheiro, A.C., Proud, S.R., Sandholt, I., 2010. Modeling angular dependences in land surface temperatures from the SEVIRI instrument onboard the geostationary meteosat second generation satellites. IEEE Trans. Geosci. Remote Sens. 48, 3123–3133.

Roujean, J.-L., 2000. A parametric hot spot model for optical remote sensing applications. Remote Sens. Environ. 71, 197–206.

Snyder, W.C., Wan, Z., Zhang, Y., Feng, Y.Z., 1998. Classification-based emissivity for land surface temperature measurement from space. Int. J. Remote Sens. 19, 2753–2774.

Trebs, I., Mallick, K., Bhattarai, N., Sulis, M., Cleverly, J., Woodgate, W., Silberstein, R., Hinko-Najera, N., Beringer, J., Meyer, W.S., 2021. The role of aerodynamic resistance in thermal remote sensing-based evapotranspiration models. Remote Sens. Environ. 264, 112602.

Trenberth, K.E., Fasullo, J.T., 2009. Global warming due to increasing absorbed solar radiation. Geophys. Res. Lett. 36.

Trigo, I.F., Ermida, S.L., Martins, J.P.A., Gouveia, C.M., Göttsche, F.-M., Freitas, S.C., 2021. Validation and consistency assessment of land surface temperature from geostationary and polar orbit platforms: SEVIRI/MSG and AVHRR/Metop. ISPRS J. Photogramm. Remote Sens. 175, 282–297.

Vinnikov, K.Y., Yu, Y., Goldberg, M.D., Tarpley, D., Romanov, P., Laszlo, I., Chen, M., 2012. Angular anisotropy of satellite observations of land surface temperature. Geophys. Res. Lett. 39, L23802.

Wan, Z., 2014. New refinements and validation of the collection-6 MODIS land-surface temperature/emissivity product. Remote Sens. Environ. 140, 36–45.

Wan, Z., Dozier, J., 1996. A generalized split-window algorithm for retrieving land-surface temperature from space. IEEE Trans. Geosci. Remote Sens. 34, 892–905.

Wang, K., Wan, Z., Wang, P., Sparrow, M., Liu, J., Zhou, X., Haginoya, S., 2005. Estimation of surface long wave radiation and broadband emissivity using moderate

resolution imaging spectroradiometer (MODIS) land surface temperature/emissivity products. J.Geophys.Res.Atmos. 110.
Wang, T., Yan, G., Chen, L., 2012. Consistent retrieval methods to estimate land surface shortwave and longwave radiative flux components under clear-sky conditions. Remote Sens. Environ. 124, 61–71.
Wang, W., Liang, S., Meyers, T., 2008. Validating MODIS land surface temperature products using long-term nighttime ground measurements. Remote Sens. Environ. 112, 623–635.
Wang, W., Liang, S., 2009. Estimation of high-spatial resolution clear-sky longwave downward and net radiation over land surfaces from MODIS data. Remote Sens. Environ. 113, 745–754.
Wang, W., Liang, S., 2010. A method for estimating clear-sky instantaneous land-surface longwave radiation with GOES sounder and GOES-R ABI data. IEEE Geosci. Remote Sens. Lett. 7, 708–712.
Wu, H., Zhang, X., Liang, S., Yang, H., Zhou, G., 2012. Estimation of clear-sky land surface longwave radiation from MODIS data products by merging multiple models. J.Geophys.Res.Atmos. 117.
Yan, G., Jiao, Z.-H., Wang, T., Mu, X., 2020. Modeling surface longwave radiation over high-relief terrain. Remote Sens. Environ. 237, 111556.
Yan, G., Wang, T., Jiao, Z., Mu, X., Zhao, J., Chen, L., 2016. Topographic radiation modeling and spatial scaling of clear-sky land surface longwave radiation over rugged terrain. Remote Sens. Environ. 172, 15–27.
Yu, S., Li, L., Cao, B., Zhang, H., Zhu, L., Xin, X., Liu, Q., 2022. Surface downward longwave radiation estimation from new generation geostationary satellite data. Atmos. Res. 106255.
Zeng, Q., Cheng, J., Dong, L., 2020. Assessment of the long-term high-spatial-resolution global land surface satellite (GLASS) surface longwave radiation product using ground measurements. IEEE J.Select. Top.Appl.Earth Observ.Remote Sens. 13, 2032–2055.